



UNIVERSIDAD DE INVESTIGACIÓN DE TECNOLOGÍA EXPERIMENTAL YACHAY

Escuela de Ciencias Químicas e Ingeniería

TÍTULO: Modeling of chiral induced spin selectivity effect under a magnetic field perturbation

Trabajo de integración curricular presentado como requisito para la
obtención del título de Químico

Autor:

Manuel Antonio Escobar Ordóñez

Tutores:

Manuel Caetano, Ph.D.

Solmar Varela, Ph.D.

Urcuquí, Enero 2022

SECRETARÍA GENERAL
(Vicerrectorado Académico/Cancillería)
ESCUELA DE CIENCIAS QUÍMICAS E INGENIERÍA
CARRERA DE QUÍMICA
ACTA DE DEFENSA No. UITEY-CHE-2022-00015-AD

A los 19 días del mes de enero de 2022, a las 16:00 horas, de manera virtual mediante videoconferencia, y ante el Tribunal Calificador, integrado por los docentes:

Presidente Tribunal de Defensa Dr. SAUCEDO VAZQUEZ, JUAN PABLO , Ph.D.

Miembro No Tutor Dra. LOPEZ GONZALEZ, FLORALBA AGGENY , Ph.D.

Tutor Dr. CAETANO SOUSA MANUEL , Ph.D.

El(la) señor(ita) estudiante **ESCOBAR ORDOÑEZ, MANUEL ANTONIO**, con cédula de identidad No. **1724815483**, de la **ESCUELA DE CIENCIAS QUÍMICAS E INGENIERÍA**, de la Carrera de **QUÍMICA**, aprobada por el Consejo de Educación Superior (CES), mediante Resolución **RPC-SO-39-No.456-2014**, realiza a través de videoconferencia, la sustentación de su trabajo de titulación denominado: **MODELING OF CHIRAL INDUCED SPIN SELECTIVITY EFFECT UNDER A MAGNETIC FIELD PERTURBATION.**, previa a la obtención del título de **QUÍMICO/A**.

El citado trabajo de titulación, fue debidamente aprobado por el(los) docente(s):

Tutor Dr. CAETANO SOUSA MANUEL , Ph.D.

Y recibió las observaciones de los otros miembros del Tribunal Calificador, las mismas que han sido incorporadas por el(la) estudiante.

Previamente cumplidos los requisitos legales y reglamentarios, el trabajo de titulación fue sustentado por el(la) estudiante y examinado por los miembros del Tribunal Calificador. Escuchada la sustentación del trabajo de titulación a través de videoconferencia, que integró la exposición de el(la) estudiante sobre el contenido de la misma y las preguntas formuladas por los miembros del Tribunal, se califica la sustentación del trabajo de titulación con las siguientes calificaciones:

Tipo	Docente	Calificación
Presidente Tribunal De Defensa	Dr. SAUCEDO VAZQUEZ, JUAN PABLO , Ph.D.	10,0
Miembro Tribunal De Defensa	Dra. LOPEZ GONZALEZ, FLORALBA AGGENY , Ph.D.	10,0
Tutor	Dr. CAETANO SOUSA MANUEL , Ph.D.	10,0

Lo que da un promedio de: **10 (Diez punto Cero)**, sobre 10 (diez), equivalente a: **APROBADO**

Para constancia de lo actuado, firman los miembros del Tribunal Calificador, el/la estudiante y el/la secretario ad-hoc.

Certifico que en cumplimiento del Decreto Ejecutivo 1017 de 16 de marzo de 2020, la defensa de trabajo de titulación (o examen de grado modalidad teórico práctica) se realizó vía virtual, por lo que las firmas de los miembros del Tribunal de Defensa de Grado, constan en forma digital.

ESCOBAR ORDOÑEZ, MANUEL ANTONIO
Estudiante

Dr. SAUCEDO VAZQUEZ, JUAN PABLO , Ph.D.
Presidente Tribunal de Defensa

Dr. CAETANO SOUSA MANUEL , Ph.D.
Tutor

Dra. LOPEZ GONZALEZ, FLORALBA AGGENY , Ph.D.
Miembro No Tutor

YEPEZ MERLO, MARIELA SOLEDAD
Secretario Ad-hoc

AUTORÍA

Yo, **Manuel Antonio Escobar Ordóñez**, con cédula de identidad **1724815483**, declaro que las ideas, juicios, valoraciones, interpretaciones, consultas bibliográficas, definiciones y conceptualizaciones expuestas en el presente trabajo; así cómo, los procedimientos y herramientas utilizadas en la investigación, son de absoluta responsabilidad de el autor del trabajo de integración curricular. Así mismo, me acojo a los reglamentos internos de la Universidad de Investigación de Tecnología Experimental Yachay.

Urcuquí, Enero del 2022.

A handwritten signature in blue ink that reads "Manuel Escobar".

Manuel Antonio Escobar Ordóñez

CI: 1724815483

AUTORIZACIÓN DE PUBLICACIÓN

Yo, **Manuel Antonio Escobar Ordóñez**, con cédula de identidad **1724815483**, cedo a la Universidad de Tecnología Experimental Yachay, los derechos de publicación de la presente obra, sin que deba haber un reconocimiento económico por este concepto. Declaro además que el texto del presente trabajo de titulación no podrá ser cedido a ninguna empresa editorial para su publicación u otros fines, sin contar previamente con la autorización escrita de la Universidad.

Asimismo, autorizo a la Universidad que realice la digitalización y publicación de este trabajo de integración curricular en el repositorio virtual, de conformidad a lo dispuesto en el Art. 144 de la Ley Orgánica de Educación Superior.

Urcuquí, Enero del 2022.

Manuel Escobar

Manuel Antonio Escobar Ordóñez

CI: 1724815483

Acknowledgements

A mis profesores Solmar Varela y Manuel Caetano, quienes me guiaron por el camino de la ciencia y de la excelencia.

Abstract

Chiral induced spin selectivity (CISS) effect refers to the preferential transmission (or transfer) of electrons with one spin orientation over the other (spin-filtering) through molecular structures having chiral symmetry. CISS effect has been considered a reachable promise for using organic materials to manipulate electron spins, and to design improved spintronic devices and new quantum materials. Furthermore, CISS effect has been found as a central mechanism behind a number of important biological phenomena. Although an extensive number of experimental arrays have been used to examine CISS, there is not a general agreement about a theoretical description that allows the effect to be fully understood and controlled.

In order to understand the CISS effect different theoretical approaches have been developed. In this work, an analytical tight-binding (TB) model and first-principles theoretical description were developed for helicene molecule, which incorporates the kinetic energy contribution and the effect of the Stark, spin-orbit (SOC) intrinsic and Zeeman interactions. We use a lowest order perturbation theory along with a matrix decimation procedure to derive the SOC, Rashba and Zeeman hamiltonian terms. According to the helicene model, the main contribution to the CISS effect comes from the Rashba coupling while the terms of the Zeeman effect are negligible small for small values of Earth's magnetic field.

Keywords: helicene, spin selectivity, tight-binding model, intrinsic spin-orbit, Stark effect, Rashba interaction, Zeeman effect.

Resumen

El efecto de selectividad de espín inducida por quiralidad (CISS por sus siglas en inglés) se refiere a la transmisión preferencial (o transporte) de electrones con una orientación de espín sobre la otra (filtrado de espín) a través de estructuras moleculares que tienen simetría quiral. El efecto CISS se ha considerado una promesa factible para el uso de materiales orgánicos para manipular los espines de electrones, para diseñar dispositivos espintrónicos mejorados y nuevos materiales cuánticos. Además, el efecto CISS se ha encontrado como un mecanismo central detrás de una serie de fenómenos biológicos importantes. Aunque se ha implementado un gran número de metodologías experimentales para examinar CISS, no existe un acuerdo general sobre una descripción teórica que permita comprender y controlar completamente el efecto. Para comprender el efecto CISS se han desarrollado diferentes enfoques teóricos. En este trabajo, se desarrolló un modelo analítico de tight-binding junto con una descripción teórica de primeros principios para la molécula heliceno. El modelo incorpora la contribución cinética y el efecto de las interacciones Stark, spin-órbita intrínseca y Zeeman. Se usó teoría de perturbación de primer orden junto con un procedimiento de decimación matricial, con el cual se derivó los términos correspondientes a spin-órbita, Rashba y Zeeman. Según el modelo del heliceno, la principal contribución al efecto CISS proviene del acoplamiento Rashba, mientras que los términos del efecto Zeeman son insignificantes para valores pequeños del campo magnético de la Tierra.

Palabras clave: heliceno, selectividad de spin, modelo de enlace fuerte, interacciones spin-orbita, efecto Stark, interacciones Rashba, efecto Zeeman.

CONTENTS

Contents	v
Introduction	1
1.1 Problem Statement	6
1.2 General and Specific Objectives	7
2 Theoretical Frame	9
2.1 Tight-binding model	9
2.2 Slater-Koster parameters and overlaps	10
2.3 Hamiltonian terms	11
2.3.1 Kinetic energy	11
2.3.2 Stark effect: external electric fields	12
2.3.3 Spin-orbit coupling interation	13
2.3.4 Magnetic Zeeman Effect	18
2.4 Decimation Procedure	20
2.5 Feynmann-type paths	22

3	Results and Discussion	24
3.1	Helicene model	24
3.2	Feynman paths that connect p_z orbitals	29
3.3	Slater-Koster overlaps for helicenenes	33
3.3.1	Hermiticity and conservation of angular momentum	37
3.4	Effective hamiltonian	40
3.5	Magnitude of the interactions	43
3.5.1	Kinetic energy hamiltonian	43
3.5.2	Spin-orbit hamiltonian	44
3.5.3	Rashba hamiltonian	46
3.5.4	Zeeman hamiltonian	47
	Conclusions	50
A	Derivation of General Overlap Expression	52
B	Derivation of the Spin-Orbit terms	55
C	Derivation of the Stark term	57
D	Derivation of the Zeeman terms	59
E	Model Parameters and Estimated Overlaps	61
	Bibliography	64

INTRODUCTION

Spintronics is a multidisciplinary field which studies the properties of the electron spin and manipulation of spin degrees of freedom in solid-state systems [1, 2]. Spin is described as intrinsic angular momentum of a particle and it is distinguished from the angular momentum due to the motion of the particle in space, called the orbital angular momentum. For particles having spin, the description of the state by means of the wave function must determine the probability of their different positions in space and possible orientations of the spin.

Some of the phenomena related to spin are spin transport in electronic materials, as well as of spin dynamics, spin relaxation [1], spin-dependent transfer processes, spin Hall effect and many others. These phenomena will likely have important technological impact in the near future, even though, as it is suggested by [3], developments in the area of spintronics are still greatly dependent on the exploration and discovery of novel material and the possibility to describe these systems.

Advances in spintronics and its applications in industry include:

- (a) Read Heads, a component of hard disk drives which flies on the surface of the disk and converts the magnetic field into electric signal and it works for sensing dense

magnetic storage media [4]. These components are highly used today in laptop computers and entertainment systems [5].

- (b) Magnetic random access memory (MRAM), which are a type of non-volatile and stand-alone memories with very high endurance and scalability [6].
- (c) Programmable spintronic logic devices based on magnetic tunnel junction elements, which have advantages in being nonvolatile, rapid, have unlimited reconfigurable variations, and low-power consumption [7].
- (d) Perimeter defense systems, magnetometers, and high current monitoring devices for power systems [5], etc.

On the other hand, spintronic devices and prototypes take advantage for being potentially faster and less power consuming equipment, since the relevant energy scale for spin dynamics is relatively small [5]. Additionally, spintronics makes use of organic materials to mediate or control spin polarized signals [8], also having the convenience of being cheap, have low-weight, be mechanically flexible, chemically interactive, and bottom-up fabricated electronics [8].

One of the most important developments in spintronics, which was aimed by the investigation of how spin-polarized electric currents can be injected into magnetic layers, led in 1988 to the discovery of the phenomenon of giant magnetoresistance (GMR) [9, 10]. This effect occur when a magnetic field reorients the magnetization in different regions of a material composed by alternating ferromagnetic/nonmagnetic layers, causing a change of the electrical resistance [4]. The ferromagnetic layer has an uneven distribution of electrons that have opposite spin directions (up and down) at equilibrium and therefore leads to a net magnetic moment which will determine the electric current in a GMR device [6]. One of the most important impacts of this effect lies on the spin valves field and their use in magnetic hard disk drives, which led researchers Albert Fert and Peter Grünberg to be awarded in 2007 with the Nobel Prize in Physics [11].

An important research field in spintronics research is the chiral induced spin selec-

tivity (CISS) effect. CISS was first reported in 1999 by Naaman and coworkers who were developing electron transmission experiments [12]. By measuring the transmission of photoelectrons through thin organized films of organic chiral molecules, it was found that the scattering probability of polarized electrons depends on the electron spin [12]. Specifically, researchers observed an enhanced scattering of one electron spin polarization relative to the other by a chiral layer of organic lysinein, which was later related to the intrinsic structure of monolayer films. Moreover, the authors determined that the principal contribution to the asymmetry in the electron scattering cross sections was due to the spin-orbit interaction. In that sense, the combination of different perturbation of the spin orbitals and the spatial wavefunctions asymmetry produce chiral electron scattering and a net helicity [12].

In this respect, the term chirality is referred to a molecule's or material's lack of parity symmetry; that is, it has no inversion symmetry, and a mirror symmetry operation transforms one enantiomer into the other [13]. This definition encloses helical structures such as helicenes and DNA. Because many biomolecules are chiral and many biochemical reactions involve chiral molecules, much attention has been deposited on understanding the inherent properties of chiral molecules, as well as the influence of chiral symmetry on other properties such as the electric and magnetic response of molecules [13]. It was not until 2011 that the definitive observation of CISS was reported by Göhler and collaborators. They observed exceptionally high spin polarization (exceeding 60%) of electrons transmitted through double-stranded DNA (dsDNA) molecules adsorbed on gold surface [14]. The most striking finding of this experiment was that molecular assemblies of chiral molecules can act as efficient spin filters for photoelectrons [14]. Therefore, the CISS effect may be defined as the transmission of electron with one preferential spin orientation over the other through the chiral axis of a molecule [15]. Hitherto, this effect has been largely demonstrated in several experimental designs [15, 16] and for a broad variety of molecular systems [17, 18, 19], and new experimental evidence involving this effect continue to be reported. Additionally, due to the CISS effect allows the creation of spin-polarized elec-

trons without the use of magnets, new prospects for spintronics is opened up [20]. By this reason, this phenomenon has motivated the development of different theoretical models to understand CISS in molecular structures. For instance, CISS effect have been established in local probe measurements such as scanning tunneling (STM) and atomic force microscopy (AFM) [21]; in molecular junctions; in electron photoemission through chiral monolayers; spin polarization effects on chemical reactions [15]; and in enantioselective response to magnetic polarization [22]. This effect has been observed in DNA [17, 23], proteins, oligopeptides [18], and helicenenes [19].

In contrast to experimental developments, theoretical attempts have also been presented to rationalize this unexpected phenomenon. The main discrepancy between the calculations and the experimental results lies in the magnitude of the spin polarization P , which may be defined as:

$$P = \frac{I_\alpha - I_\beta}{I_\alpha + I_\beta} \quad (1.1)$$

for which I_α and I_β are the experimental measurables (e.g., current, rate constant, etc.) for spin pointing parallel or antiparallel to the electron's velocity [24] (see Fig. 1.1). While spin polarization exceeding 80% is obtained experimentally, most models and calculations produce polarizations of only a few percent [24], and as a result they underestimate the magnitude of the CISS effect by several orders of magnitude. For this reason, it has been suggested and it is broadly accepted that CISS is related to a combination of enhanced intrinsic SOC due to a breaking of spatial inversion symmetry by spin processes [22]. Even though, a consistent theory is not yet constructed. Recent evidence suggests the possible importance of spin selectivity in the biochemistry and biology areas, which are even extended to play a role on bird and fish navigation by the Earth's magnetic field [25]. For instance, it has been undoubtedly documented the presence of a magnetic compass system in birds [26, 27]. Nevertheless, the mechanisms that allow migratory birds to orient in the geomagnetic field have long time remained inexplicable [26, 27, 28]. In that sense, a few proposals have been suggested, being one the radical pair mechanism which includes spin-chemical processes [28, 29]. However, spin selective filtering by chiral molecules may

also contribute to this phenomenon [25]. Thus, it would be significant to test the influence of the geomagnetic field on a chiral molecule and hence to determine possible spin filtering processes.

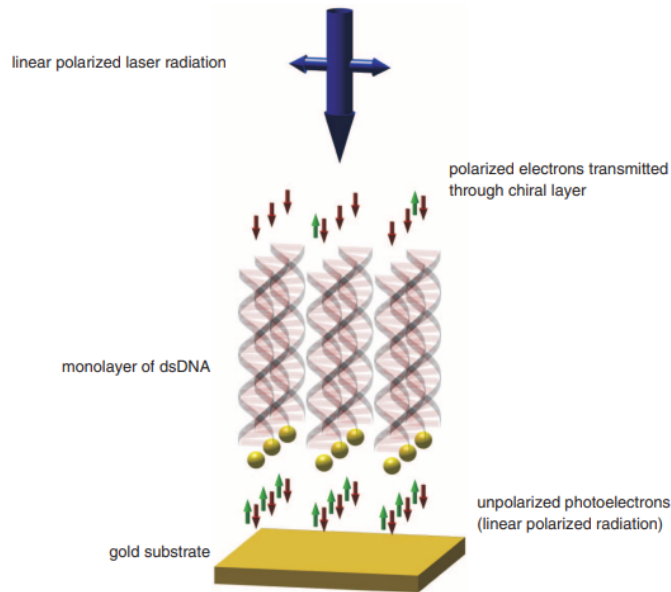


Figure 1.1: A scheme describing the monolayer of DNA as spin filter. Unpolarized electrons are ejected from the gold substrate and most of the polarized electrons are transmitted through the DNA with spin aligned antiparallel to their velocity. Retrived from Naaman and Waldeck [13].

In that sense, an important case of study are helicenes, which are pure carbon based system with chiral properties due their helicity and have been shown to display a CISS effect [19]. Helicenes present two properties that may make them good candidates for CISS: (i) chirality of the helix (either left- or right-handed) and (ii) potentially moderate or even strong SOC [30]. Therefore, the helicene structure can display spin selectivity which arise from its helical symmetry and subsequent intrinsic SOC [19]. Moreover, this phenomenon may be enhanced by electric or magnetic fields which can change the spin polarization and create other type of electronic couplings.

Thus, it would be desirable to model a simple system yet containing the essential

physics necessary for the description of helicenes structures under electrical and magnetic effects. In many cases, density functional theory (DFT) is used to analyze electronic structures having low computational cost and high accuracy [31], yet it cannot isolate the contribution of each atomic interaction effect. A powerful method for this purpose is the analytical tight-binding (TB) models incorporating first-principles theoretical description. This method allows the possibility to analyse the results in terms of various parameters inherent of the system, such as SOC, Rashba and Zeeman strengths, spin polarization, various symmetries etc. Additionally, the tight-binding model is a semiclassical method which enables the incorporation of material-specific parameters which provide an easy way to tune and simplify the physical description while reproducing the real behaviour of the system. Moreover, this method allows to perform a lot of comparatively fast calculations in combination with freedom to vary the many interactions the system can involve. Finally, the detailed tight-binding analysis can yield the connection between molecule's chirality and the various interaction effects such as the intrinsic SOC and electric/magnetic fields.

For this work purpose, analytical tight-binding (TB) models and first-principles theoretical description incorporating both kinetic and intrinsic SOC contributions as well as Rashba-type interactions, have been developed for helix systems [17, 19].

1.1 Problem Statement

The main problem is that there is no a consistent description of the CISS effect, which opens discussion about the fundamental mechanism and the magnitude of physical parameters which can be included to describe CISS. Even though most of the proposed models so far agree in that a part of the CISS effect is due to the presence of a intrinsic spin-orbit coupling along molecular helical structures, a full theory is not yet constructed. Along with the CISS effect, there is an interest to determine the mechanism by which some birds orientate in the geomagnetic field, and if it is caused by spin selectivity of chiral molecules present in the animal organism. These two problems can be enclosed by the unknown

magnitude of CISS and the unknown effect of the geomagnetic field on biological systems, and if these two are correlated.

The precise topic that this research will address is to understand the effect of an external magnetic field over chiral molecules, namely helicenes. Additionally, the combination of other magnetic and electric effects as well as different electronic couplings will be analyzed.

The novelty of this work relies in the methodology used to solve the problem of the chiral helicene molecule: a matrix decimation which includes the effect of SOC, Stark and weak external magnetic fields.

1.2 General and Specific Objectives

The general objective of this work is to develop a three-dimensional analytic tight binding model of helicenes capable to identify and rationalize the possible effect of internal and external interactions, namely intrinsic spin-orbit coupling, Stark electric effect, and Zeeman magnetic effect. The specific objectives are:

1. Perform a geometrical description and relate physical parameters to the helicene structure.
2. Describe the interaction effects of helicenes and their physical behavior in electric and magnetic fields.
3. Derive Slater-Koster elements that connect first nearest neighbors and relate them to structural parameters of helicenes.
4. Analyze spin processes through effective Feynman paths.

5. Derive the effective Hamiltonian of the helices which incorporates spin-orbit, Rashba and magnetic couplings using the matrix decimation approach of band folding.
6. Find analytical expressions for the energy corrections corresponding to the spin-orbit, Rashba and magnetic contributions.

CHAPTER 2

THEORETICAL FRAME

In this chapter is explained the theoretical background used in this work to obtain the subsequent results.

2.1 Tight-binding model

The tight-binding hamiltonian describes the electronic structure in terms of localized electrons orbitals which interact only with nearest neighbours atoms and are modestly perturbed from their isolated atomic form [32]. Moreover, depending on the solid and if the orbitals are well localized (as long as electrons interact strongly with the atoms), it is possible to neglect the atomic orbital overlaps and potentials between atoms more than one or two lattice spacings apart. Of course, the fundamental interactions are kept to first neighbors. This strategy is based on the linear combination of atomic orbitals (LCAO) method developed by Bloch [33], which describes the orbitals using an appropriate atomic-orbital like basis set. In general, the tight-binding method works by writing the eigenstates of the hamiltonian in an atomic-like basis set, $\{\phi_{\mathbf{r}\alpha}\}$ where \mathbf{r} is denoted by the position index of the atomic site and $\alpha = |l, m\rangle$ denotes the type of orbital (both the orbital l and magnetic

quantum numbers of the atomic state), e.g., $2s$, $2p_x$, $2p_y$ [32, 34, 35]. In this formulation, the representation of solids and molecules eigenstates, or indeed any states, becomes:

$$\psi_n(\mathbf{r}) = \sum_{\alpha,l} a_{\alpha l} \phi_{\alpha l}(\mathbf{r}). \quad (2.1)$$

where $a_{\alpha l}$ are expansion coefficients.

The tight-binding model can include all kind of interactions that determine the way electrons couple throughout a molecule to produce its properties [36]. As a consequence, the method allows to formulate analytical expressions for the perturbations included in a system such as the intrinsic spin-orbit (SO) coupling, Stark, and Zeeman effects. In that sense, these quantities can be obtained from a matrix decimation procedure of band folding that connects nearest neighbor sites. Additionally, the tight binding model enable the incorporation of material-specific parameters which provide an easy way to tune and simplify the physical description to reproduce the real behaviour of the system. Hence, effectiveness of this method is due to its ability to deal with systems of low symmetry, lacking periodicity, or having complex unit cells [32], being particularly useful for the study of large unit cell systems such as the case of helices.

2.2 Slater-Koster parameters and overlaps

The Slater-Koster overlap terms represent the extent at which orbital wavefunctions overlap in a given geometrical configuration. In this work, it is only considered two-center atomic interactions with atomic orbitals of the form $Y_{l,m_l} = |l, m_l\rangle$ with Y the spherical harmonics functions, l representing the angular momentum quantum number (e.g. $l = s, p, d$ orbitals) and m_l the magnetic quantum number (e.g. $m_l = \sigma, \pi, \delta$ bonds). Then the overlap integral between two orbitals located at the positions \mathbf{R}_i and \mathbf{R}_j is:

$$E_{\mu\nu}^{ij} = \langle l, m, \mathbf{R}_i | \mathbf{H} | l', m', \mathbf{R}_j \rangle = \int d^3\mathbf{r} \mu_{l,m}(\mathbf{r} - \mathbf{R}_i) \mathbf{H} \nu_{l',m'}(\mathbf{r} - \mathbf{R}_j), \quad (2.2)$$

where \hat{H} is the hamiltonian for the bond energy and $E_{\mu\nu}^{ij}$ is the Slater-Koster overlap energy, which is evaluated with respect the interatomic distance $\mathbf{R}_j - \mathbf{R}_i$, that is, the

vector that connects the two atoms in the positions \mathbf{R}_i and \mathbf{R}_j . Due to the selection rules, the magnetic quantum numbers m_l and m'_l of the atomic orbitals must be the same [37]. Moreover, if $\mu = \nu$ the Slater-Koster overlap will represent the contribution to the on-site energies due to existence of other atoms, while if $\mu \neq \nu$ then the overlap represent the hopping-element on-site from $\nu \rightarrow \mu$ due to existence of other atoms [37].

2.3 Hamiltonian terms

For a system, the hamiltonian can be written in the general form by:

$$\mathbf{H} = \mathbf{H}_K + \mathbf{H}_S + \mathbf{H}_{SO} + \mathbf{H}_Z, \quad (2.3)$$

where \mathbf{H}_K is the kinetic energy contribution, \mathbf{H}_S the Stark interaction, and \mathbf{H}_{SO} and \mathbf{H}_Z are the spin-orbit intrinsic and Zeeman interactions, respectively.

2.3.1 Kinetic energy

In general, the hamiltonian describes the dynamics of a particular system among the orbitals of the model [36]. Equation (2.4) shows the lowest-order kinetic term, which involves only wavefunction overlaps between p_z orbitals, and are expressed by the coupling term t . Hence, all other type of overlaps and atom interactions are taken as perturbations to this energy. That is, the presence of other atoms sites produce a shifting or splitting of the energies associated to this site [38]. Moreover, the kinetic overlaps depend on the step angle between carbon atoms in the helicene and the pitch of the helix, having both σ and π bonding contributions. In in second quantization formulation, the kinetic term can be represented as:

$$\mathbf{H}_K = \sum_k t^k \sum_{(i,j)} a_i^\dagger a_j, \quad (2.4)$$

where a_i^\dagger creates an electron in the atom site i while a_j annihilates an electron on the atom site j . In this case, the second-quantized notation is used only for algebraic convenience

and in fact, the second quantized hamiltonian is the same as the molecular N-electron hamiltonian [37].

2.3.2 Stark effect: external electric fields

The Stark effect explains the change in the energy levels of an atom caused by a uniform external electric field. Thus, the term associated with it, called Stark term, represents the extra energy of the nucleus and electron in the external field. For an electric field in the z direction, the hamiltonian corresponding to the Stark term is:

$$\mathbf{H}_S = -eE_z\hat{z} = -eE_zr\cos(\theta), \quad (2.5)$$

where e is the charge of the electron, E_z is the strength of and external electric field \mathbf{E} along the z direction, and \hat{z} is the unit vector. It is assumed that the electric field does not depend on the position, it to say, it is constant in all space. In spherical coordinates, θ represents the angle between \mathbf{E} and z , with r the radial coordinate. The Stark perturbation is odd with respect parity inversion [39], thus, the only non-vanishing matrix elements are those for opposite parity states. In specific, the only non-zero element is:

$$\mathbf{H}_S = 3ea_0E_z \equiv \xi_{sp}, \quad (2.6)$$

where a_0 is the Bohr radius, e is the electron elementary charge and ξ_{sp} is the magnitude of the electric interaction between p and s orbitals. Then, the Stark matrix elements can be summarized in Table 2.1 as:

Table 2.1: Stark matrix elements between s and p orbitals.

	$ s\rangle$	$ p_x\rangle$	$ p_y\rangle$	$ p_z\rangle$
$\langle s $	0	0	0	ξ_{sp}
$\langle p_x $	0	0	0	0
$\langle p_y $	0	0	0	0
$\langle p_z $	ξ_{sp}	0	0	0

For example, considering an electric field of $E_z = 25$ V/nm, the electric magnitude is $\xi_{sp} = 10.5$ eV.

2.3.3 Spin-orbit coupling interaction

The atomic spin-orbit coupling (SOC) arises from the interaction between the coulombic potential of a nucleus and the electron intrinsic magnetic moment orbiting that nucleus [40]. Thus, the spin-orbit term corresponds to the magnetic interaction that couples the spin magnetic momentum with the orbital angular momentum, but only for the optically active electrons [41]. Another way to understand this term is by the interaction of the spin magnetic moment with the magnetic field which is “felt” by the electron due to its motion around the nucleus [42].

Then, considering that the electron is moving at a velocity \mathbf{v} in the electrostatic field \mathbf{E} created by the proton, a magnetic field \mathbf{B} appears in the electron frame, which is given by [42]:

$$\mathbf{B} = -\left(\frac{\mathbf{v}}{c^2}\right) \times \mathbf{E}, \quad (2.7)$$

where $\mathbf{v} = \mathbf{p}/m_e$, being \mathbf{p} the momentum of the electron with effective mass m_e . Additionally, each electron possesses an intrinsic magnetic moment $\boldsymbol{\mu}_S$ which can interact with the field \mathbf{B} . In specific, the magnetic moment generated by the electron is: [43]:

$$\boldsymbol{\mu}_S = \frac{e}{m_e} \mathbf{S}, \quad (2.8)$$

where e and \mathbf{S} are the charge and spin of the electron, respectively. Then, the corresponding SOC interaction energy is expected to be:

$$\mathbf{H}_{\text{SOC}} = -\boldsymbol{\mu}_S \cdot \mathbf{B}. \quad (2.9)$$

Next, consider a central potential energy $V(r) = \phi(r)$ [40], which includes the contributions of both the electrically charged nucleus and the negatively charged electron cloud

in the inner shells [43]. Hence, the electrostatic energy associated to this potential is [40]:

$$\mathbf{E} = -\nabla\phi = -\frac{\mathbf{r}}{r}\frac{\partial V}{\partial r}, \quad (2.10)$$

which is obtained by expressing the gradient in spherical coordinates. Here, \mathbf{r} is the vector position at which the field points out and r is the magnitude of such vector. By replacing Eqs. (2.7) and (2.8) in (2.9), the SOC hamiltonian becomes:

$$\begin{aligned} \mathbf{H}_{\text{SOC}} &= \left(\frac{e}{m_e}\mathbf{S}\right) \left(\frac{\mathbf{v}}{c^2} \times \mathbf{E}\right) \\ &= -\left(\frac{e}{m_e}\mathbf{S}\right) \left[\frac{\mathbf{p}}{m_e c^2} \times \frac{\mathbf{r}}{r} \frac{dV}{dr}\right], \\ &= \frac{e}{m_e^2 c^2} \frac{1}{r} \frac{\partial V}{\partial r} \mathbf{L} \cdot \mathbf{S} \end{aligned} \quad (2.11)$$

where the fact that $\mathbf{L} = -\mathbf{p} \times \mathbf{r}$ was used. However, a relativistic correction arises due to the Thomas precession [40], which corrects the energy by a factor of 1/2:

$$\mathbf{H}_{\text{SOC}} = \frac{e}{2m_e^2 c^2} \frac{1}{r} \frac{\partial V}{\partial r} \mathbf{L} \cdot \mathbf{S}. \quad (2.12)$$

Hence, the SOC term can be expressed in the following ways:

$$\begin{aligned} \mathbf{H}_{\text{SOC}} &= \frac{e}{2m_e^2 c^2} \frac{1}{r} \frac{\partial V}{\partial r} \mathbf{L} \cdot \mathbf{S} \\ &= -\frac{e\hbar}{4m_e^2 c^2} \mathbf{S} \cdot (\mathbf{p} \times \nabla V) \\ &= \lambda \mathbf{L} \cdot \mathbf{S}. \end{aligned} \quad (2.13)$$

where λ is a known function of the position r .

2.3.3.1 Spin-Orbit Overlaps

The SOC term contributes in the spin-orbit SO interaction that connects two different sites in a molecular structure. To compute the SOC contribution, it is required both a “good” basis selection and a corresponding orbital representation. On the other hand,

when the λ position dependence is taken into account, \mathbf{L} and \mathbf{S} no longer commute with the total hamiltonian [42]. This result in the following relations:

$$\begin{aligned} [L_z, \mathbf{H}_{\text{SOC}}] &= \lambda[L_z, L_x S_x + L_y S_y + L_z S_z] = \lambda[i\hbar L_y S_x - i\hbar L_x S_y] \\ [S_z, \mathbf{H}_{\text{SOC}}] &= \lambda[S_z, L_x S_x + L_y S_y + L_z S_z] = \lambda[i\hbar L_x S_y - i\hbar L_y S_x]. \end{aligned} \quad (2.14)$$

Thus, it is necessary to find a constant of motion which commute with the hamiltonian. For this purpose, it is defined $\mathbf{J} = \mathbf{L} + \mathbf{S}$ as the total angular momentum, which satisfies the commutation relation [42]:

$$[J_z, \mathbf{H}_{\text{SOC}}] = [L_z + S_z, \mathbf{H}_{\text{SOC}}] = 0. \quad (2.15)$$

Considering only the unperturbed hamiltonian or bare $E_{\mu\nu}^{ij}$ elements, it is possible to work with any of the following complete set of commuting observables (CSCO) [43]:

$$\begin{aligned} \text{Set 1: } \{L^2, S^2, L_z, S_z\}, \\ \text{Set 2: } \{L^2, S^2, J^2, J_z\}. \end{aligned} \quad (2.16)$$

Thus, a state can be determined by specifying the quantum numbers, j , l , s , m_j , m_l , and m_s , which are connected with the eigenvalues of angular momentum operators through [39]:

$$\begin{aligned} J^2 &= j(j+1)\hbar^2 & J_z &= m_j\hbar \\ L^2 &= l(l+1)\hbar^2 & \text{and } L_z &= m_l\hbar \\ S^2 &= s(s+1)\hbar^2 & S_z &= m_s\hbar. \end{aligned} \quad (2.17)$$

Once the CSCO is chosen, in this case Set 1, it is important to select the adequate ket vectors which represent both the s and p orbitals. The bare p orbitals expressed in the ket form $|l, m_l\rangle$, are [17]:

$$\begin{aligned} |p_x\rangle &= -\frac{1}{\sqrt{2}}(|1, 1\rangle - |1, -1\rangle) \\ |p_y\rangle &= -\frac{i}{\sqrt{2}}(|1, 1\rangle + |1, -1\rangle) \\ |p_z\rangle &= |1, 0\rangle. \end{aligned} \quad (2.18)$$

Then, expanding the ket $|l, m_l\rangle$ in the spin space so that $|l, m_l; s, m_s\rangle$ expresses the spin dependence of the original ket, it is obtained:

$$\begin{aligned}
|p_x \uparrow\rangle &= -\frac{1}{\sqrt{2}} \left(\left| 1, 1; \frac{1}{2}, \frac{1}{2} \right\rangle - \left| 1, -1; \frac{1}{2}, \frac{1}{2} \right\rangle \right) \\
|p_x \downarrow\rangle &= -\frac{1}{\sqrt{2}} \left(\left| 1, 1; \frac{1}{2}, -\frac{1}{2} \right\rangle - \left| 1, -1; \frac{1}{2}, -\frac{1}{2} \right\rangle \right) \\
|p_y \uparrow\rangle &= -\frac{1}{\sqrt{2}} \left(\left| 1, 1; \frac{1}{2}, \frac{1}{2} \right\rangle + \left| 1, -1; \frac{1}{2}, \frac{1}{2} \right\rangle \right) \\
|p_y \downarrow\rangle &= -\frac{1}{\sqrt{2}} \left(\left| 1, 1; \frac{1}{2}, -\frac{1}{2} \right\rangle + \left| 1, -1; \frac{1}{2}, -\frac{1}{2} \right\rangle \right) \\
|p_z \uparrow\rangle &= \left| 1, 0; \frac{1}{2}, \frac{1}{2} \right\rangle \\
|p_z \downarrow\rangle &= \left| 1, 0; -\frac{1}{2}, -\frac{1}{2} \right\rangle.
\end{aligned} \tag{2.19}$$

The kets presented in 2.19 can be expressed in a couple basis via a Clebsch-Gordan transformation. For this, it is necessary to refer to the right Clebsch-Gordan transformation matrix: because all p orbitals possess $l = 1$ and electron spin possesses $s = 1/2$, the required matrix have $(l, s) = (1, 1/2)$, see Eq. (2.20).

$$\begin{array}{cc}
& \begin{array}{cccccc} \frac{3}{2} & \frac{3}{2} & \frac{1}{2} & \frac{3}{2} & \frac{1}{2} & \frac{3}{2} \end{array} \\
& \begin{array}{cccccc} \frac{3}{2} & \frac{1}{2} & \frac{1}{2} & -\frac{1}{2} & -\frac{1}{2} & -\frac{3}{2} \end{array} \\
\begin{array}{cc} 1 & \frac{1}{2} \\ 1 & -\frac{1}{2} \\ 0 & \frac{1}{2} \\ 0 & -\frac{1}{2} \\ -1 & \frac{1}{2} \\ -1 & -\frac{1}{2} \end{array} & \left(\begin{array}{c|ccc|c} 1 & & & & & \\ \hline & \sqrt{\frac{1}{3}} & \sqrt{\frac{2}{3}} & & & \\ & \sqrt{\frac{2}{3}} & -\sqrt{\frac{1}{3}} & & & \\ \hline & & & \sqrt{\frac{2}{3}} & \sqrt{\frac{1}{3}} & \\ & & & \sqrt{\frac{1}{3}} & -\sqrt{\frac{2}{3}} & \\ \hline & & & & & 1 \end{array} \right).
\end{array} \tag{2.20}$$

In specific, a Clebsch-Gordan transformation matrix is composed of rows having (m_l, m_s) uncoupled coefficients and columns composed of $\binom{j}{m_j}$ coupled coefficients. Then,

it is possible to transform from either coupled or uncoupled base to the other. In this case, starting from the p orbital uncoupled ket $|l, m_l; s, m_s\rangle$, it can be obtained the corresponding coupled ket in the form $|j, m_j\rangle$. After performing the correct transformation, the p orbitals become:

$$\begin{aligned}
|p_x \uparrow\rangle &= -\frac{1}{\sqrt{2}} \left(\left| \frac{3}{2}, \frac{3}{2} \right\rangle - \sqrt{\frac{1}{3}} \left| \frac{3}{2}, \frac{1}{2} \right\rangle + \sqrt{\frac{2}{3}} \left| \frac{1}{2}, -\frac{1}{2} \right\rangle \right) \\
|p_x \downarrow\rangle &= -\frac{1}{\sqrt{2}} \left(\sqrt{\frac{1}{3}} \left| \frac{3}{2}, \frac{1}{2} \right\rangle + \sqrt{\frac{2}{3}} \left| \frac{1}{2}, \frac{1}{2} \right\rangle - \left| \frac{3}{2}, -\frac{3}{2} \right\rangle \right) \\
|p_y \uparrow\rangle &= \frac{i}{\sqrt{2}} \left(\left| \frac{3}{2}, \frac{3}{2} \right\rangle + \sqrt{\frac{1}{3}} \left| \frac{3}{2}, \frac{1}{2} \right\rangle - \sqrt{\frac{2}{3}} \left| \frac{1}{2}, -\frac{1}{2} \right\rangle \right) \\
|p_y \downarrow\rangle &= \frac{i}{\sqrt{2}} \left(\sqrt{\frac{1}{3}} \left| \frac{3}{2}, \frac{1}{2} \right\rangle + \sqrt{\frac{2}{3}} \left| \frac{1}{2}, \frac{1}{2} \right\rangle + \left| \frac{3}{2}, -\frac{3}{2} \right\rangle \right) \\
|p_z \uparrow\rangle &= \sqrt{\frac{2}{3}} \left| \frac{3}{2}, \frac{1}{2} \right\rangle - \sqrt{\frac{1}{3}} \left| \frac{1}{2}, \frac{1}{2} \right\rangle \\
|p_z \downarrow\rangle &= \sqrt{\frac{2}{3}} \left| \frac{3}{2}, -\frac{1}{2} \right\rangle + \sqrt{\frac{1}{3}} \left| \frac{1}{2}, -\frac{1}{2} \right\rangle
\end{aligned} \tag{2.21}$$

Finally, the different SOC matrix elements involving p orbitals given in Eq. (2.21) are summarized in Table 2.2.

Table 2.2: SOC matrix elements between p orbitals.

	$ p_x\rangle$	$ p_y\rangle$	$ p_z\rangle$
$\langle p_x $	0	$-i\mathbf{s}_z\xi_p$	$i\mathbf{s}_y\xi_p$
$\langle p_y $	$i\mathbf{s}_z\xi_p$	0	$-i\mathbf{s}_x\xi_p$
$\langle p_z $	$-i\mathbf{s}_y\xi_p$	$i\mathbf{s}_x\xi_p$	0

where $\xi_p = \lambda\hbar/2$ is the magnitude of the SOC interaction for p orbitals ($\xi_p \sim 6$ meV for carbon atoms [19, 23]), and \mathbf{s}_z represent the Pauli matrices in a rotating coordinate

system, and in this case, for the helicene. Explicitly, they are represented by:

$$\begin{aligned} \mathbf{s}_x &= \sigma_X \cos(\phi_i) + \sigma_Y \sin(\phi_i) \\ \mathbf{s}_y &= -\sigma_X \cos(\phi_i) + \sigma_Y \sin(\phi_i) \\ \mathbf{s}_z &= \sigma_Z \end{aligned} \quad (2.22)$$

with XYZ being the global coordinate system presented in Fig. 2.1.

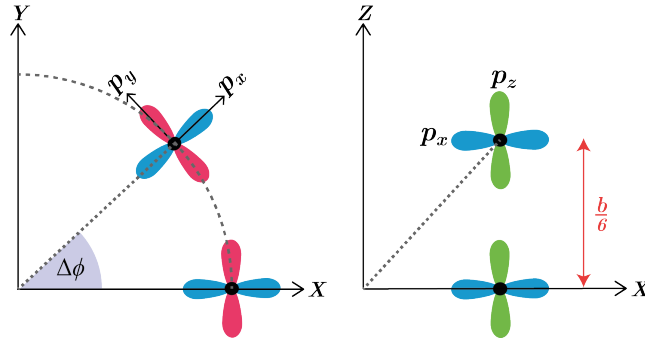


Figure 2.1: Structure of the helicene model in the XY and XZ plane, showing the orientation of p_x (blue colored), p_y (red) and p_z orbitals (green).

2.3.4 Magnetic Zeeman Effect

The Zeeman effect explains the splitting of energy levels of an atom due to the potential energy created by the atom magnetic dipole orientation in an applied external magnetic field [41]. This field interacts with the various magnetic moments present in the atom namely the electron orbital $\boldsymbol{\mu}_L$ and spin magnetic moments $\boldsymbol{\mu}_s$, and also the magnetic moment of the nucleus $\boldsymbol{\mu}_I$ [42]. Explicitly, these terms are:

$$\boldsymbol{\mu}_L = \frac{e}{2m_e} \mathbf{L} \quad ; \quad \boldsymbol{\mu}_s = \frac{e}{m_e} \mathbf{S} \quad ; \quad \boldsymbol{\mu}_I = -\frac{qg_p}{2M_p} \mathbf{I}. \quad (2.23)$$

where g_p , q , and M_p are the Landé g-factor, charge and mass of the proton, respectively.

It is important to note that these magnetic moments only appear for optically active electrons. Here, optical electrons are referred to the electrons which determine the total angular momentum of an atom by means of L-S or J-J coupling [41]. Other electrons in a

completely filled subshell do not present net magnetic dipole moments and hence can be neglected [41].

As the Zeeman hamiltonian describes the interaction energy of the atom with the magnetic field \mathbf{B} , it can be written as the sum [42]:

$$\begin{aligned}\mathbf{H}_Z &= -(\boldsymbol{\mu}_L + \boldsymbol{\mu}_S + \boldsymbol{\mu}_I) \cdot \mathbf{B} \\ &= \frac{e}{2m_e}(\mathbf{L} + 2\mathbf{S}) + \frac{qg_p}{2M_p}\mathbf{I}.\end{aligned}\tag{2.24}$$

According to the Born–Oppenheimer approximation [42], the nucleus has a much larger mass compared to the electron ($M_p \gg m_e$), and thus the last term in Eq. (2.24) can be neglected. Moreover, if \mathbf{B} is set in the z direction ($\mathbf{B} = B\hat{\mathbf{z}}$), then:

$$\mathbf{H}_Z = \frac{e}{2m_e}(L_z + 2S_z).\tag{2.25}$$

In this work, it is considered external magnetic fields of the magnitude of the Earth, so this field is not strong enough to disturb the coupling $\mathbf{J} = \mathbf{L} + \mathbf{S}$. In other words, the Zeeman effect is small compared to the SOC effect and hence in the weak-field limit, the ket base of SOC effect can be used, see Eq. (2.10). This is because the external magnetic field “is weak compared to the internal atomic magnetic fields that couple \mathbf{S} and \mathbf{L} to form \mathbf{J} and only causes a relatively slow precession of \mathbf{S} about the direction of \mathbf{B} ” [41]. For this case, the only non vanishing term is:

$$\mathbf{H}_Z = -\frac{3}{2}\mu_B B_z i \equiv \mu_p,\tag{2.26}$$

where μ_B is the Bohr magneton and μ_p is defined as the magnitude of the external magnetic interaction for p orbitals. Finally, the only non-vanishing terms for the Zeeman effect can be represented in matrix form as shown in Table 2.3.

Considering that the borh magneton values is $\mu_B = 5.788 \times 10^{-5}$ eV/T and that the Earth's magnetic field varies from 25 to 60 μT [44], then the magnetic term results in $\mu_p = 3.47 \times 10^{-9}$ eV at the maximum value of B_z , but also it is possible to include another contribution for the magnetic field, in form of an external one.

Table 2.3: Zeeman matrix elements between p orbitals.

	$ p_x\rangle$	$ p_y\rangle$	$ p_z\rangle$
$\langle p_x $	0	$i\mu_p$	0
$\langle p_y $	$i\mu_p$	0	0
$\langle p_z $	0	0	0

2.4 Decimation Procedure

The decimation method is based on the renormalization group techniques of statistical mechanics [45], which has been proven to be very powerful in providing concise and compact descriptions of the collective behavior of many-body systems [46]. The decimation procedure allows reducing a general $N \times N$ hamiltonian into a 2×2 effective hamiltonian which catch the essential physical behavior of the studied system. This effective hamiltonian exhibits modified as well as new couplings due to a priori exact elimination of degrees of freedom [46]. Also, these couplings indicates how the presence of other sites has the effect of shifting or splitting the energies of a particular site [38]. To illustrate this, consider the following hamiltonian:

$$H = \begin{pmatrix} \varepsilon_1 & t & r \\ t & \varepsilon_2 & s \\ r & s & \varepsilon_3 \end{pmatrix}, \quad (2.27)$$

where ε_i represent the in site energy at position i and t with s represent the different couplings between the sites. In this case, all the entries are real values. The corresponded eigenvalue problem $\varepsilon\Psi(u_1, u_2, u_3) = H\Psi(u_1, u_2, u_3)$ can be expressed with the set of linear equations:

$$\begin{aligned} \varepsilon u_1 &= \varepsilon_1 u_1 + t u_2 + r u_3 \\ \varepsilon u_2 &= \varepsilon_2 u_2 + t u_1 + s u_3 \\ \varepsilon u_3 &= \varepsilon_3 u_3 + r u_1 + s u_2 \end{aligned} \quad (2.28)$$

To reduce the hamiltonian dimension, one start by choosing a square submatrix H_χ containing the unperturbed energies. The selection of this submatrix depends on physical considerations: for instance for electronic transport, only the free electrons in the system will contribute the most. In graphene-like structures, these electrons are found in the out-of-plane orbitals, which are commonly denoted as the p_z orbitals. Hence, the submatrix H_χ shall contain the aforementioned p_z orbital overlaps to represent correctly the electron transport. The other coupled matrices are redefined as [23]:

$$H = \begin{pmatrix} H_\gamma & T \\ T^\dagger & H_\chi \end{pmatrix} \quad (2.29)$$

where the new matrices having the new couplings correspond to:

$$H_\gamma = \begin{pmatrix} \varepsilon_1 & t \\ t & \varepsilon_1 \end{pmatrix} \quad ; \quad H_\chi = \varepsilon_3 \quad ; \quad T = \begin{pmatrix} t \\ r \end{pmatrix} \quad ; \quad T = \begin{pmatrix} t & r \end{pmatrix}. \quad (2.30)$$

It is important to notice that the decimation works perfectly for complex-valued matrices as long as the matrix hermiticity is satisfied. For real valued and symmetric matrices, this is clearly the case. To continue the decimation process, the minor H_χ is inverted. Finally, a decimated hamiltonian can be obtained by carrying the following product of matrices:

$$H_{\text{eff}} = S^{-1/2} [H_\gamma - T H_\chi^{-1} T^\dagger] S^{-1/2}, \quad (2.31)$$

where $S = 1 - T H_\chi^{-1} T^\dagger$ is an orthogonal projector on the system's state space. In this approximation, $S \sim 1$ [23, 47], so the decimated hamiltonian becomes:

$$H \approx H_\gamma - T H_\chi^{-1} T^\dagger. \quad (2.32)$$

and for the given example, equation 2.32 allows to obtain the effective hamiltonian:

$$H_{\text{eff}}(\varepsilon) = \begin{pmatrix} \varepsilon_1 + \frac{r^2}{\varepsilon - \varepsilon_3} & t + \frac{rs}{\varepsilon - \varepsilon_3} \\ t + \frac{rs}{\varepsilon - \varepsilon_3} & \varepsilon_2 + \frac{s^2}{\varepsilon - \varepsilon_3} \end{pmatrix}. \quad (2.33)$$

The effective hamiltonian obtained satisfies the equation $\det(\varepsilon \mathbf{1} - H_{\text{eff}}(\varepsilon)) = 0$. It can be noticed that in general, the decimation reduces the hamiltonian dimension at the

expense of generating non-linear renormalized coefficients, namely the inverse dependence on the energy variable ε [38]. However, the effective hamiltonian can be further linearized in a region of interest by keeping the higher order terms according to the Feynmann-type paths.

2.5 Feynmann-type paths

In 1948, Feynman published different approach to quantum mechanics which still gave the same results from Schrödinger equation [48]. The main essence in this formulation is to assign a probability amplitude to each possible trajectories that connect two space-time points [49]. In this sense, each possible trajectory has the same probability weight [49], but since each path has a different action, they contribute with a different phase [43]. Then, the contributions from all possible trajectories are sum up to obtain the transition amplitude between the two space-time points [49]. This also can be seen as a “perturbation series”, since each path may has different kind of interactions which “perturbs” the free propagation of the particle [50].

The Feynman formulation do not require a detailed description of the behavior of each particle in the system, but rather just the average behavior of one or two physical particles [50], such as the electron. This formulation can be used to give a physical interpretation of the ways or paths that connect two sites in a molecular structure. These paths may be evaluated approximately by selecting the most important terms in it. This is because the probability of a electron going from p_z^i to p_z^j by means of merely kinetic energy (electronic hopping matrix elements) is larger compared to the probabilities which includes various perturbation interactions. In other words, the kinetic Slater-Koster terms are larger compared to the Stark, spin-orbit, Rashba and Zeeman terms. Then, higher order terms will give successively smaller contributions, and thus the solution can be approximated by summing the series up to the first- or second-order terms [50]. It is

important to note that in this context, the order of the term is referred to the total number of interactions that appear in a certain path [50].

In the next section, it will be shown the effective paths that an electron can take in going from one atomic orbital to another. Correspondingly, these paths are derived between the effective couplings of p_z orbitals, which are the same orbitals in which the decimation procedure was carried out.

CHAPTER 3

RESULTS AND DISCUSSION

In this section are derived the Slater-Koster overlaps for the helicene structure and it is verified the hermiticity and angular momentum conservation of these terms. Next, the total hamiltonian is constructed from the Slater-Koster overlaps and the orbital interaction arising from the Stark, intrinsic SOC, Rashba coupling and Zeeman effects. Then, the total hamiltonian is decimated using a matricial approach. Finally the magnitude for each type of interaction is obtained.

3.1 Helicene model

Helicenes are non-planar polycyclic aromatic molecules composed by orthofused benzene or other aromatic rings [51]. The terminal rings repel each other and produce steric hindrance which cause helicenes to fold along the helical axis. Additionally, helicenes have a C₂-symmetric axis perpendicular to the helical axis (see Fig. 3.1) which makes them chiral despite not having asymmetrical carbons nor chiral centers [51].

In this work, the helicene structure is taken to be a right-handed circular helix. For our purposes, the helicenes will be considered as consisting of only carbon atoms so any

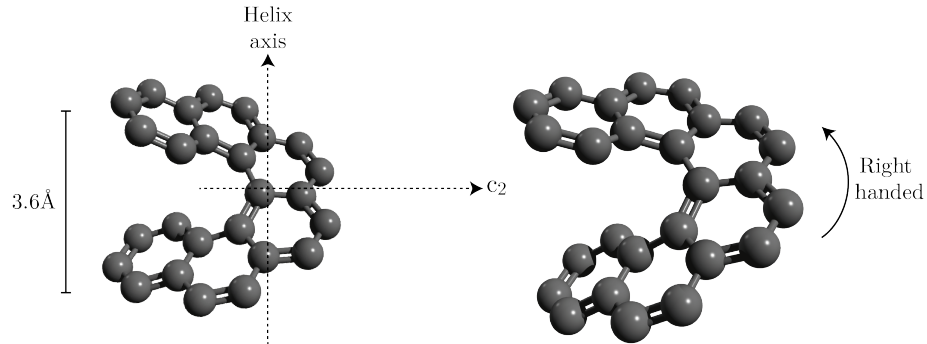


Figure 3.1: Atomistic structure of 6-Helicene with right handed helicity.

hydrogen contribution is neglected. In fact, the polarization of the hydrogen bond may result in strong internal electric fields (different from the ones produced by atomic cores) which in turn can produce a considerable Stark coupling [47]. Also, it has been speculated that hydrogen bonding may be responsible for the largest spin activity observed in biological chiral molecules [47]. Therefore, the hydrogen bonds may not be completely negligible. However, instead of considering the possible polarization of the hydrogen bonds, only a Stark coupling in the z -direction is considered.

Another approximation is to neglect the resonance of the aromatic double bonds in the helicene, so all distances between carbon atoms are equidistant. As a matter of fact, the tight-binding theory make use of localized basis functions [37] and thus it cannot account directly for the electron delocalisation that results from the aromatic resonance. However, the strength of the σ and π bonding can be adjusted using the values of the Slater-Koster parameters V_{pp}^{π} which are inherent to each atom-type [17, 23]. Despite the helicene is a finite structure, it is better to work with an infinite helix so that the molecule will be composed of only 4 inequivalent atoms as is shown in Fig. 3.2. Thus, these 4 inequivalent atoms constitute the unit cell of the helicene, and they will be the only atoms needed to model the whole system. It should be noted that even though the outer atoms seems to be equivalent, the handedness of the helix provokes these atoms to be mirror images of each other.

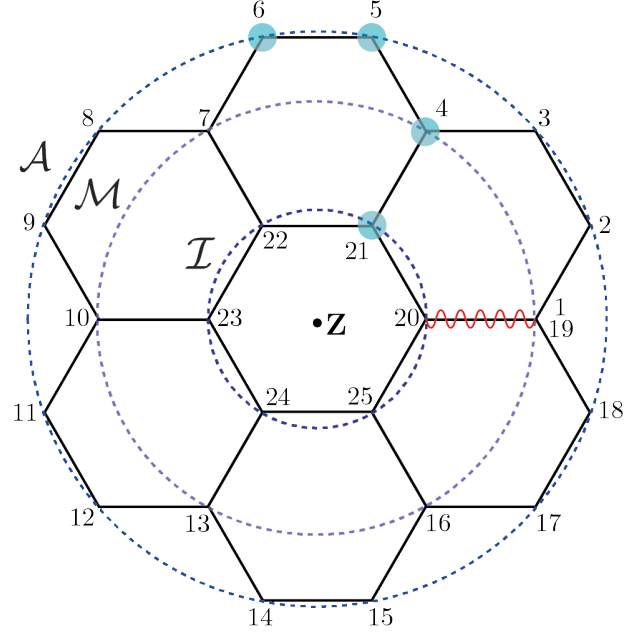


Figure 3.2: Top view of right handed helicene divided into three concentric helices (\mathcal{I} , \mathcal{M} , and \mathcal{A}). Inequivalent atom sites are marked with blue circles. Wavy red curve indicates that no bonding in plane is formed.

In addition, helicenes are formed by three concentric helices: an inner helix, denoted as \mathcal{I} , with radius $r_0 = a_0 \sim 1.4 \text{ \AA}$; a middle helix \mathcal{M} with $r_1 = 2a_0$; and an outer helix \mathcal{A} with $r_2 = a_1 = \sqrt{7}a_0$. The angle between two neighboring sites on the inner helix is $\phi_0 = \pi/3$ while the angle for nearest neighbors on the outer helix is $\phi_2 = 2 \arcsin(1/(2\sqrt{7})) \approx 21.8^\circ$ as seen in Fig. 3.2. The last angle is defined between nearest neighbour atoms in the middle and outer helices and its value is $\phi_1 = \frac{1}{2}(\frac{\pi}{3} - \phi_2) \approx 19.1^\circ$. Finally, the pitch of the helicene which is the height of a complete helix turn is 3.6 \AA and it will be denoted by b .

On the other hand, the orientation of the orbitals presented in this work is based on the previous description of the helicene structure made by Geyer et. al [19]. Based on this reference, each atom site has its own right-handed local coordinate system. Also, the local z -axis is taken to be parallel to the global Z -axis while the local x -axis is normal to the cylinder surface as shown in Fig. 3.3. Thus, these orbitals form a local system at each site, and they may vary from different atoms.

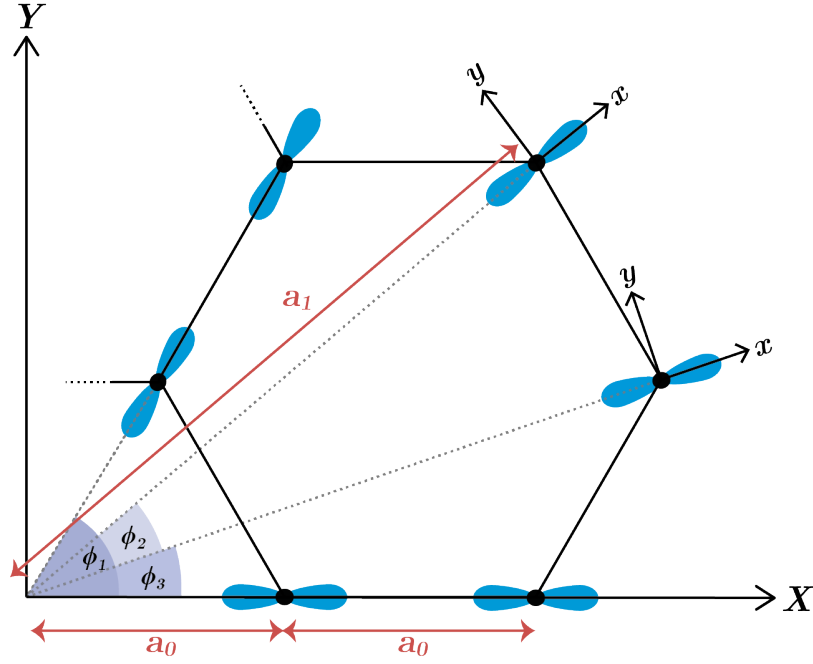


Figure 3.3: Global reference system (X,Y) and the orientation of p_x orbitals in the helicene in the local system (x,y). For a convenient visualization, only a single in-plane p orbital is drawn on each carbon site.

Furthermore, to characterize each atom in the solid state system, two vectors are required which correspond to the position of the atoms in the molecule (atom position vector) and the direction of a set of orbitals at that site (orbital direction vector). In this regard, the position of the atom is the distance to a specified origin while the orbital direction can be parametrized with respect to that origin. In particular, it is convenient to represent the vector position of a helicene carbon atom on site i in cylindrical coordinates as:

$$\mathbf{R}_i = \left(R_i \cos(\Phi_i), R_i \sin(\Phi_i), \frac{b}{2\pi} \Phi_i \right), \quad (3.1)$$

where R_i is one of the three radii defined in 3.2 and Φ_i is a sum of multiples of ϕ_0 , ϕ_1 and ϕ_2 (see Fig. 3.3 for reference). In this case, the helicene pitch is represented by b .

Explicitly, the radial and angular dependencies are:

$$R_i = \begin{cases} r_0 & \text{for } i \in \mathcal{N} \\ r_1 & \text{for } i \in \mathcal{M} \\ r_2 & \text{for } i \in \mathcal{A} \end{cases} \quad \text{and} \quad \Phi_i = \begin{cases} (1-i)\phi_0 & \text{for } i \in \mathcal{N} \\ (1-i)\phi_1 & \text{for } i \in \mathcal{M} \cup \mathcal{A} \\ (1-i)\phi_2 & \text{for } i \in \mathcal{A} \end{cases} \quad (3.2)$$

Based on previous tight-binding models [17, 19, 23, 52], for two carbon atoms at sites i and j , the Slater-Koster overlaps are given by the expression:

$$H_{\mu\nu}^{ij} = \langle \mathbf{n}(\mu_{ij})^{\parallel}, \mathbf{n}(\nu_{ji})^{\parallel} \rangle V_{\mu\nu}^{\sigma} + \langle \mathbf{n}(\mu_{ij})^{\perp}, \mathbf{n}(\nu_{ji})^{\perp} \rangle V_{\mu\nu}^{\pi}, \quad (3.3)$$

where $\mathbf{n}(\mu_i)$ is a unit vector in the direction of the orbital μ_i and \parallel denotes a projection of $\mathbf{n}(\mu_i)$ onto the interatomic distance $\mathbf{R}_{ji} = \mathbf{R}_j - \mathbf{R}_i$, while \perp denotes a projection onto a plane perpendicular to \mathbf{R}_{ji} . In any case, these formulas contemplate only mathematical notions such as the inner product and thus they are not constructed to be Hermitian nor conserve angular momentum. However, the system can be further constrained to satisfy both these conditions (see discussion in Sec. 2.3.1).

Besides, $\mathbf{n}(\mu_{ij})^{\parallel}$ and $\mathbf{n}(\nu_{ji})^{\perp}$ allow to adjust the Slater-Koster parameters to the geometry of a given molecule and in this case, helicenes. Redefining the unitary vectors with their vector projection on the helicene interatomic distance, and considering that an orbital in an arbitrary direction can be decomposed into a parallel and perpendicular component such that $\mathbf{n}(\mu_i) = \mathbf{n}(\mu_{ij})^{\parallel} + \mathbf{n}(\mu_{ij})^{\perp}$, the orbital vectors become:

$$\mathbf{n}(\mu_{ij})^{\parallel} = \begin{cases} \frac{\langle \mathbf{R}_{ji}, \mathbf{n}(\mu_i) \rangle}{\|\mathbf{R}_{ji}\|^2} \mathbf{R}_{ji}, & \text{for } \mu \in (x, y, z) \\ \frac{\mathbf{R}_{ji}}{\|\mathbf{R}_{ji}\|}, & \text{for } \mu = s \end{cases} \quad (3.4)$$

and

$$\mathbf{n}(\mu_{ij})^{\perp} = \begin{cases} \mathbf{n}(\mu_i) - \frac{\langle \mathbf{R}_{ji}, \mathbf{n}(\mu_i) \rangle}{\|\mathbf{R}_{ji}\|^2} \mathbf{R}_{ji}, & \text{for } \mu \in (x, y, z) \\ 0, & \text{for } \mu = s. \end{cases} \quad (3.5)$$

Replacing the projections given in Eqs. (3.4) and (3.5) into (3.3), it can be obtained a general prescription to compute orbital overlaps (see Appendix A). For overlaps involving only p orbitals, the matrix elements are:

$$H_{\mu\nu}^{ij} = \langle \mathbf{n}(\mu_i), \mathbf{n}(\nu_j) \rangle V_{\mu\nu}^\sigma + \frac{\langle \mathbf{R}_{ji}, \mathbf{n}(\nu_j) \rangle \langle \mathbf{R}_{ji}, \mathbf{n}(\mu_i) \rangle}{\|\mathbf{R}_{ji}\|^2} (V_{\mu\nu}^\sigma - V_{\mu\nu}^\pi), \quad (3.6)$$

and for overlaps involving s and p orbitals, the matrix elements are:

$$H_{\mu\nu}^{ij} = \frac{\langle \mathbf{R}_{ij}, \mathbf{n}(\nu_j) \rangle}{\|\mathbf{R}_{ij}\|} V_{\mu\nu}^\sigma. \quad (3.7)$$

Finally, to compute the Slater-Koster overlaps it is required an appropriate orbital parametrization. In this matter, local system of each p orbital will be also treated in cylindrical coordinates:

$$\begin{aligned} \mathbf{n}(x_i) &= (\cos(\Phi_i), \sin(\Phi_i), 0), \\ \mathbf{n}(y_i) &= (-\sin(\Phi_i), \cos(\Phi_i), 0), \\ \mathbf{n}(z_i) &= (0, 0, 1), \end{aligned} \quad (3.8)$$

where Φ_i is the same angle defined in the carbon position vector. That is, both the atom position and the orbital direction vectors are parametrized with the same angles to further simplify calculations. In that sense, Eq. (3.3) can be used to compute the different atom overlaps in helicenes, which in turn will depend on geometric parameters given by Eq. (3.2).

3.2 Feynman paths that connect p_z orbitals

The different paths give a “map” to keep track of all the sequences of interaction that the electron can have in going from one site to another [50]. In this case, these type of interactions are given by: a purely kinetic term associated with the Slater-Koster elements contribution ($H_{\mu\nu}^{ij}$), an electric term (ξ_{sp}) due to the Stark effect contribution, an intrinsic magnetic term (ξ_p) due to the spin-orbit coupling, a Rashba contribution (proportional to $\xi_p \xi_{sp}$) due to the orbital coupling by the SOC and Stark interactions, and finally, an external magnetic term (μ_p) due to the Zeeman effect contribution.

The effective electron pathways connecting an initial p_z orbital to another p_z orbital are summarized in Table 3.1. These paths include different combination of the aforementioned kinetic, electric and magnetic interactions. Some of these paths produce a spin-flip and will be named as spin active processes.

Table 3.1: First order possible paths that connects p_z^i to p_z^j

$p_z^i \xleftrightarrow{E_{zz}^{ij}} p_z^j$
$p_z^i \xleftrightarrow{\xi_{sp}} s^i \xleftrightarrow{E_{sz}^{ij}} p_z^j$
$p_z^i \xleftrightarrow{\xi_p} p_x^i \xleftrightarrow{E_{xz}^{ij}} p_z^j$
$p_z^i \xleftrightarrow{\xi_p} p_y^i \xleftrightarrow{E_{yz}^{ij}} p_z^j$
$p_z^i \xleftrightarrow{\xi_p} s^i \xleftrightarrow{E_{sx}^{ij}} p_x^j \xleftrightarrow{\xi_{sp}} p_z^j$
$p_z^i \xleftrightarrow{\xi_p} s^i \xleftrightarrow{E_{sy}^{ij}} p_y^j \xleftrightarrow{\xi_{sp}} p_z^j$
$p_z^i \xleftrightarrow{E_{zs}^{ij}} s^j \xleftrightarrow{\xi_{sp}} p_x^j \xleftrightarrow{\xi_p} p_z^j$
$p_z^i \xleftrightarrow{E_{zs}^{ij}} s^j \xleftrightarrow{\xi_{sp}} p_y^j \xleftrightarrow{\xi_p} p_z^j$
$p_z^i \xleftrightarrow{\xi_p} p_x^i \xleftrightarrow{\mu_p} p_y^i \xleftrightarrow{E_{yz}^{ij}} p_z^j$
$p_z^i \xleftrightarrow{\xi_p} p_y^i \xleftrightarrow{\mu_p} p_x^i \xleftrightarrow{E_{xz}^{ij}} p_z^j$
$p_z^i \xleftrightarrow{\xi_p} p_x^i \xleftrightarrow{\mu_p} p_y^i \xleftrightarrow{E_{ys}^{ij}} s^j \xleftrightarrow{\xi_{sp}} p_z^j$
$p_z^i \xleftrightarrow{\xi_p} p_x^i \xleftrightarrow{\mu_p} p_y^i \xleftrightarrow{\xi_{sp}} s^i \xleftrightarrow{E_{sz}^{ij}} p_z^j$
$p_z^i \xleftrightarrow{\xi_p} p_y^i \xleftrightarrow{\mu_p} p_x^i \xleftrightarrow{E_{xs}^{ij}} s^j \xleftrightarrow{\xi_{sp}} p_z^j$

The lowest order paths that effectively connect two p_z orbitals are:

(1) The kinetic term:

$$p_z^i \xleftrightarrow{E_{zz}^{ij}} p_z^j \quad (3.9)$$

which connects p_z orbitals at different sites by means of the kinetic E_{zz}^{ij} element and it is shown in Fig. 3.4.

(2) The first-order Stark coupling:

$$p_z^i \xleftrightarrow{\xi_{sp}} s^i \xleftrightarrow{E_{sz}^{ij}} p_z^j \quad (3.10)$$

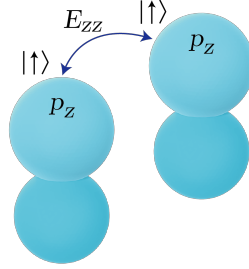


Figure 3.4: Kinetic path due to p_z - p_z overlaps between nearest neighbors. The process is not spin active (spin states are indicated at the end of blue arrows).

which combines the Stark coupling between a s and a p_z orbital in the same site and the nearest neighbour overlap by the E_{sz}^{ij} element and the process is depicted in Fig. 3.5.

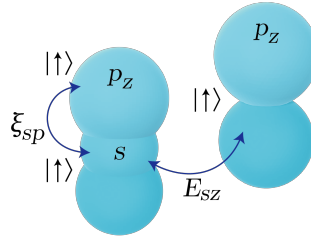


Figure 3.5: The external electric field along the z axis couples p_z and s orbitals on the same site. Then the overlap E_{sz} enables nearest neighbor hopping to another p_z orbital. The process is not spin active.

(3) The first-order intrinsic SO:

$$\begin{aligned}
 p_z^i &\xleftrightarrow{\xi_p} p_x^i \xleftrightarrow{E_{xz}^{ij}} p_z^j \\
 p_z^i &\xleftrightarrow{\xi_p} p_y^i \xleftrightarrow{E_{yz}^{ij}} p_z^j
 \end{aligned} \tag{3.11}$$

which includes the in-site SOC coupling of different p orbitals and the overlaps of the form E_{pp} at different sites. Notice that the SOC coupling is referred to the coupling between p orbitals (see Table 2.2), while the intrinsic SO refers to the interaction which includes the SOC term. Also, note that ξ_p is the magnitude of the SOC interaction and is the same for any p orbital coupling. The lowest-order SO path is shown in Fig.3.6.

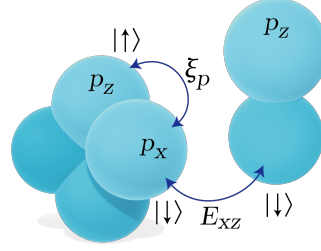


Figure 3.6: SO path couples in-site p_z orbitals and produces a spin flip transfer. The matrix element E_{xz} allows the hopping between nearest s and p orbitals. This process is spin active.

(4) The first-order Rashba coupling:

$$\begin{aligned}
 p_z^i &\xleftrightarrow{\xi_p} s^i \xleftrightarrow{E_{sx}^{ij}} p_x^j \xleftrightarrow{\xi_{sp}} p_z^j \\
 p_z^i &\xleftrightarrow{\xi_p} s^i \xleftrightarrow{E_{sy}^{ij}} p_y^j \xleftrightarrow{\xi_{sp}} p_z^j \\
 p_z^i &\xleftrightarrow{E_{zs}^{ij}} s^j \xleftrightarrow{\xi_{sp}} p_x^j \xleftrightarrow{\xi_p} p_z^j \\
 p_z^i &\xleftrightarrow{E_{zs}^{ij}} s^j \xleftrightarrow{\xi_{sp}} p_y^j \xleftrightarrow{\xi_p} p_z^j
 \end{aligned} \tag{3.12}$$

which includes a combination of the electric Stark effect, the SOC interactions, and the kinetic overlap involving E_{sp} type-elements. The lowest-order Rashba path is shown in Fig. 3.7.

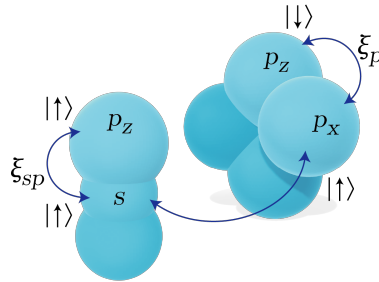


Figure 3.7: Lowest-order Rashba coupling which involves a combination of Stark and SOC interactions and $s - p_{x,y}$ overlaps. The process is spin active.

(5) The first-order Zeeman coupling:

$$\begin{aligned}
p_z^i &\xleftrightarrow{\xi_p} p_x^i \xleftrightarrow{\mu_p} p_y^i \xleftrightarrow{E_{yz}^{ij}} p_z^j \\
p_z^i &\xleftrightarrow{\xi_p} p_y^i \xleftrightarrow{\mu_p} p_x^i \xleftrightarrow{E_{xz}^{ij}} p_z^j \\
p_z^i &\xleftrightarrow{\xi_p} p_x^i \xleftrightarrow{\mu_p} p_y^i \xleftrightarrow{E_{ys}^{ij}} s^j \xleftrightarrow{\xi_{sp}} p_z^j \\
p_z^i &\xleftrightarrow{\xi_p} p_x^i \xleftrightarrow{\mu_p} p_y^i \xleftrightarrow{\xi_{sp}} s^i \xleftrightarrow{E_{sz}^{ij}} p_z^j \\
p_z^i &\xleftrightarrow{\xi_p} p_y^i \xleftrightarrow{\mu_p} p_x^i \xleftrightarrow{E_{xs}^{ij}} s^j \xleftrightarrow{\xi_{sp}} p_z^j
\end{aligned} \tag{3.13}$$

which combines the Stark, SOC, magnetic (internal and external effects) and kinetic terms. The lowest-order Zeeman path is shown in Fig. 3.8.

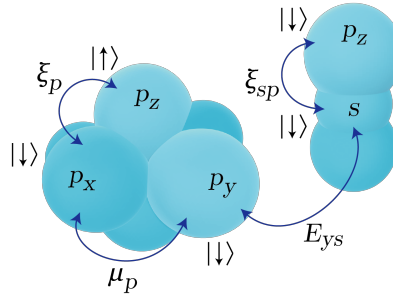


Figure 3.8: Lowest-order Zeeman coupling as a combination of Stark, SOC and magnetic Zeeman interactions, including $s - p_{x,y}$ kinetic hoppings. The process is spin active.

As seen from Figs. 3.4 to 3.8, only the paths that include the SOC term, that is ξ_p , are spin active. On the other hand, the kinetic and the Stark terms conserve the electron spin, and thus they do not flip the spin.

3.3 Slater-Koster overlaps for helices

Considering the general prescription to calculate different overlaps according to Eq. (3.2) and the geometry of helices given in Eq. (3.3), it can be obtained the expressions of all possible overlaps between the orbitals s , p_x , p_y and p_z . In particular, the Slater-Koster scheme produces any combination of two arbitrary rotating orbitals to transform into

an orbital in the direction of the interatomic distance. Even though the orientation of one selected atom may be arbitrary, it is not trivial the relative orientation of the other orbitals (nearest neighbors) with respect to the selected one. That is, choosing a reference system is not trivial. In this case, the orbital reference system is parametrized following the prescription given by Geyer et. al [19]. Additionally, Slater Koster overlaps depend on the wavefunction overlaps relative to a geometrical arrangement, and in this case, helical structure of Helicenes. For sake of simplicity, we limited our analysis by only considering overlaps between σ and π type bonds. Thus, $E_{\mu\nu}^{ij}$ will only depend on linear combinations of V_{ss}^σ , V_{sp}^σ , V_{pp}^σ and V_{pp}^π .

It is convenient to divide all possible overlaps in two groups which correspond to the σ - and π -structure. First, the matrix elements which involve only σ bonds are:

$$E_{sx}^{ij} = \frac{(\mathbf{R}_j - \mathbf{R}_i \cos(\Phi_j - \Phi_i))}{\|R_{ji}\|} V_{sx}^\sigma = E_{xs}^{ji}, \quad (3.14)$$

$$E_{xs}^{ij} = \frac{(\mathbf{R}_j \cos(\Phi_j - \Phi_i) - \mathbf{R}_i)}{\|R_{ji}\|} V_{xs}^\sigma = E_{sx}^{ji}, \quad (3.15)$$

$$E_{sy}^{ij} = \frac{\mathbf{R}_i \sin(\Phi_j - \Phi_i)}{\|R_{ji}\|} V_{sy}^\sigma = E_{ys}^{ji}, \quad (3.16)$$

$$E_{ys}^{ij} = \frac{\mathbf{R}_j \sin(\Phi_j - \Phi_i)}{\|R_{ji}\|} V_{ys}^\sigma = E_{sy}^{ji} = E_{sy}^{ij}, \quad (3.17)$$

$$E_{sz}^{ij} = \frac{b(\Phi_j - \Phi_i)}{2\pi\|R_{ji}\|} V_{sz}^\sigma = E_{zs}^{ji}, \quad (3.18)$$

$$E_{zs}^{ij} = \frac{b(\Phi_j - \Phi_i)}{2\pi\|R_{ji}\|} V_{zs}^\sigma = E_{sz}^{ji}. \quad (3.19)$$

where \mathbf{R}_i and Φ_i are defined as 3.2 and 3.3, respectively. Also, b stands for the helicene pitch.

Next, the π -structure involve both σ and π bonds. Thus, the atoms overlaps are a linear combination of V_{pp}^σ and V_{pp}^π .

$$\begin{aligned} E_{xx}^{ij} &= \cos(\Phi_j - \Phi_i) V_{xx}^\pi + \frac{(\mathbf{R}_j \cos(\Phi_j - \Phi_i) - \mathbf{R}_i) (\mathbf{R}_j - \mathbf{R}_i \cos(\Phi_j - \Phi_i))}{\|R_{ji}\|^2} (V_{xx}^\sigma - V_{xx}^\pi) \\ &= E_{xx}^{ji}, \end{aligned} \quad (3.20)$$

$$E_{yy}^{ij} = \cos(\Phi_j - \Phi_i) V_{yy}^\pi + \frac{\mathbf{R}_j \mathbf{R}_i \sin^2(\Phi_j - \Phi_i)}{\|R_{ji}\|^2} (V_{yy}^\sigma - V_{yy}^\pi) = E_{yy}^{ji}, \quad (3.21)$$

$$E_{zz}^{ij} = V_{zz}^\pi + \frac{b^2(\Phi_j - \Phi_i)^2}{4\pi^2 \|R_{ji}\|^2} (V_{zz}^\sigma - V_{zz}^\pi) = E_{zz}^{ji}, \quad (3.22)$$

$$\begin{aligned} E_{xy}^{ij} &= -\sin(\Phi_j - \Phi_i) V_{xy}^\pi + \frac{(\mathbf{R}_j \cos(\Phi_j - \Phi_i) - \mathbf{R}_i) (\mathbf{R}_i \sin(\Phi_j - \Phi_i))}{\|R_{ji}\|^2} (V_{xy}^\sigma - V_{xy}^\pi) \\ &= E_{yx}^{ji}, \end{aligned} \quad (3.23)$$

$$\begin{aligned} E_{yx}^{ij} &= \sin(\Phi_j - \Phi_i) V_{yx}^\pi + \frac{(\mathbf{R}_j \sin(\Phi_j - \Phi_i)) (\mathbf{R}_j - \mathbf{R}_i \cos(\Phi_j - \Phi_i))}{\|R_{ji}\|^2} (V_{yx}^\sigma - V_{yx}^\pi) \\ &= E_{xy}^{ji}, \end{aligned} \quad (3.24)$$

$$E_{xz}^{ij} = \frac{b(\mathbf{R}_j \cos(\Phi_j - \Phi_i) - \mathbf{R}_i) (\Phi_j - \Phi_i)}{2\pi \|R_{ji}\|^2} (V_{xz}^\sigma - V_{xz}^\pi) = E_{zx}^{ji}, \quad (3.25)$$

$$E_{zx}^{ij} = \frac{b(\Phi_j - \Phi_i) (\mathbf{R}_j - \mathbf{R}_i \cos(\Phi_j - \Phi_i))}{2\pi \|R_{ji}\|^2} (V_{zx}^\sigma - V_{zx}^\pi) = E_{xz}^{ji}, \quad (3.26)$$

$$E_{yz}^{ij} = \frac{b\mathbf{R}_j \sin(\Phi_j - \Phi_i) (\Phi_j - \Phi_i)}{2\pi \|R_{ji}\|^2} (V_{yz}^\sigma - V_{yz}^\pi) = E_{zy}^{ji}, \quad (3.27)$$

$$E_{zy}^{ij} = \frac{b(\Phi_j - \Phi_i) \mathbf{R}_i \sin(\Phi_j - \Phi_i)}{2\pi \|R_{ji}\|^2} (V_{zy}^\sigma - V_{zy}^\pi) = E_{yz}^{ji}. \quad (3.28)$$

A further simplification occur when $\mathbf{R}_i = \mathbf{R}_j$, it is to say, when $i, j \in \mathcal{I}$ or $i, j \in \mathcal{A}$ for nearest neighbours. Thus, new equalities arise and the overlap matrix elements become:

$$E_{sx}^{ij} = \frac{a(1 - \cos(\Phi_j - \Phi_i))}{\|R_{ji}\|} V_{sx}^\sigma = E_{xs}^{ij} = E_{xs}^{ji}, \quad (3.29)$$

$$E_{sy}^{ij} = \frac{a \sin(\Phi_j - \Phi_i)}{\|R_{ji}\|} V_{sy}^\sigma = -E_{ys}^{ij} = E_{ys}^{ji}, \quad (3.30)$$

$$E_{sz}^{ij} = \frac{b(\Phi_j - \Phi_i)}{2\pi \|R_{ji}\|} V_{sz}^\sigma = -E_{zs}^{ij} = E_{zs}^{ji}, \quad (3.31)$$

$$E_{xx}^{ij} = \cos(\Phi_j - \Phi_i) V_{xx}^\pi - \frac{4a^2 \sin^4\left(\frac{(\Phi_j - \Phi_i)}{2}\right)}{\|R_{ji}\|^2} (V_{xx}^\sigma - V_{xx}^\pi) = E_{xx}^{ji}, \quad (3.32)$$

$$E_{yy}^{ij} = \cos(\Phi_j - \Phi_i) V_{yy}^\pi + \frac{a^2 \sin^2(\Phi_j - \Phi_i)}{\|R_{ji}\|^2} (V_{yy}^\sigma - V_{yy}^\pi) = E_{yy}^{ji}, \quad (3.33)$$

$$E_{zz}^{ij} = V_{zz}^\pi + \frac{b^2(\Phi_j - \Phi_i)^2}{4\pi^2 \|R_{ji}\|^2} (V_{zz}^\sigma - V_{zz}^\pi) = E_{zz}^{ji}, \quad (3.34)$$

$$\begin{aligned}
E_{xy}^{ij} &= -\sin(\Phi_j - \Phi_i) V_{xy}^\pi - \frac{2a \sin^2\left(\frac{(\Phi_j - \Phi_i)}{2}\right) \sin(\Phi_j - \Phi_i)}{\|R_{ji}\|^2} (V_{xy}^\sigma - V_{xy}^\pi) \\
&= -E_{yx}^{ij} = E_{yx}^{ji},
\end{aligned} \tag{3.35}$$

$$E_{xz}^{ij} = -\frac{2ab \sin^2\left(\frac{(\Phi_j - \Phi_i)}{2}\right) (\Phi_j - \Phi_i)}{2\pi \|R_{ji}\|^2} (V_{xz}^\sigma - V_{xz}^\pi) = -E_{xz}^{ij} = E_{zx}^{ji}, \tag{3.36}$$

$$E_{yz}^{ij} = \frac{ab \sin(\Phi_j - \Phi_i) (\Phi_j - \Phi_i)}{2\pi \|R_{ji}\|^2} (V_{yz}^\sigma - V_{yz}^\pi) = E_{zy}^{ij} = E_{zy}^{ji}. \tag{3.37}$$

It should be noted that Eqs. (3.29) to (3.37) have the same form as the ones derived for DNA [17, 23] and oligopeptides [18]. This is because these structures have a similar atomic/base distribution compared to the helices couplings in either the inner helix \mathcal{I} and outer \mathcal{I} helix.

On the other hand, when $\Phi_i = \Phi_j$, that is, when $i, j \in \mathcal{I} \cup \mathcal{M}$, the only non-vanishing matrix elements are:

$$E_{sx}^{ij} = V_{sx}^\sigma = E_{xs}^{ij} = E_{xs}^{ji}, \tag{3.38}$$

$$E_{xx}^{ij} = V_{xx}^\pi = E_{xx}^{ji}, \tag{3.39}$$

$$E_{yy}^{ij} = V_{yy}^\pi = E_{yy}^{ji}, \tag{3.40}$$

$$E_{zz}^{ij} = V_{zz}^\pi = E_{zz}^{ji}. \tag{3.41}$$

It should be pointed that all these matrix elements obey the rule $V_{l,l'} = (-1)^{l+l'} V_{l',l}$ where $l = 1$ for p orbitals and $l = 0$ for s orbitals.

Up to here, it is clear that the helix helical geometry, curvature and torsion effects will affect the magnitude of the different electronic couplings. This is because the matrix elements $E_{\mu\nu}^{ij}$ depend on geometrical parameters such as the step angle between different sites in the helices and the pitch that separates them. Now, it is written explicitly the magnitude of the interatomic distance, or equivalently $\|R_{ji}\|^2$, for different helices and couplings. In general, it can be shown that:

$$\|R_{ji}\|^2 = \mathbf{R}_j^2 + \mathbf{R}_i^2 - 2\mathbf{R}_j \mathbf{R}_i \cos(\Phi_j - \Phi_i) + \frac{b^2}{4\pi} (\Phi_j^2 - \Phi_i^2) \tag{3.42}$$

Therefore, the magnitude of the interatomic distance for different helices and couplings become:

$$\|R_{ji}\|^2 = \begin{cases} 2a_0^2(1 - \cos(\Phi_j - \Phi_i)) + \frac{b^2}{4\pi}(\Phi_j^2 - \Phi_i^2) & \text{for } i, j \in \mathcal{I} \\ 2a_1^2(1 - \cos(\Phi_j - \Phi_i)) + \frac{b^2}{4\pi}(\Phi_j^2 - \Phi_i^2) & \text{for } i, j \in \mathcal{A} \\ \Phi_j - \Phi_i & \text{for } i, j \in \mathcal{I} \cup \mathcal{M} \\ 4a_0^2 + a_1^2 - 4a_0a_1 \cos(\Phi_j - \Phi_i) + \frac{b^2}{4\pi}(\Phi_j^2 - \Phi_i^2) & \text{for } i \in \mathcal{M} \cup \mathcal{A} \end{cases} \quad (3.43)$$

which can be rewritten using the angular dependence for nearest neighbours in each helix as follows:

$$\|R_{ji}\|^2 = \begin{cases} 2a_0^2(1 - \cos(\phi_0)) + \frac{b^2}{4\pi^2}\phi_0^2 & \text{for } i, j \in \mathcal{I} \\ 2a_1^2(1 - \cos(\phi_2)) + \frac{b^2}{4\pi^2}\phi_2^2 & \text{for } i, j \in \mathcal{A} \\ 0 & \text{for } i, j \in \mathcal{I} \cup \mathcal{M} \\ 4a_0^2 + a_1^2 - 4a_0a_1 \cos(\phi_1) + \frac{b^2}{4\pi^2}\phi_1^2 & \text{for } i, j \in \mathcal{M} \cup \mathcal{A} \end{cases} \quad (3.44)$$

3.3.1 Hermiticity and conservation of angular momentum

Any operator that represents a physically measurable quantity has real eigenvalues, as they are the only possible results of precise measurement of that quantity [39]. The hamiltonian represents the physical observable of the energy, and thus it is an hermitian operator.

The hermitian adjoint of a matrix \hat{H} , denoted as \hat{H}^\dagger , is the matrix obtained by interchanging rows and columns and taking the complex conjugate of each element [39]. This condition is summarized in that $\hat{H} = \hat{H}^\dagger$ [53] where \dagger indicates the complex or hermitian adjoint. Therefore, the matrix elements satisfy the condition $H_{kl} = H_{lk}^*$ [53] where $*$ indicates the complex conjugate. As a consequence, any term that appears in the hamiltonian must be hermitian, a condition that the Slater-Koster elements indeed satisfy. This hermiticity condition is reflected by interchanging both the site and position labels at the same time (e.g. $E_{sx}^{ij} = E_{xs}^{ji}$). In that sense, the hermiticity guarantees electron time

reversal, that is, the electron returns from the same place where it came from with the same probability. This traduces to that every state has a corresponded time-reversed state and the operator that transforms between these states preserves all probabilities values, thus leaving invariant the total value of any inner product between states [40]. Moreover, the time reversal implies that the initial and final states of a system are interchanged when the time development is reversed with all physical processes running backwards [40].

However, invariance under time reversal does not lead to any conservation law [40], and thus the hamiltonian hermiticity is not a sufficient but a necessary condition. Additionally, the matrix elements of the hamiltonian must conserve the total angular momentum. This condition appears between matrix elements which involves the same combination of position and orbital labels (e.g. E_{sx}^{ij} , E_{xs}^{ij} , E_{sx}^{ji} and E_{xs}^{ji}). These elements must conserve the amplitude because their difference only relies on how the electron sees the rotating orbitals (clockwise or anti-clockwise). Additionally, the overlaps involves the same orbitals only changing their relative positions.

This lead to two interpretations. The first interpretation, called Interpretation 1, is that Eqs. (3.14) to (3.28) apply with no further correction. To clarify this interpretation, consider all possible overlaps between s and p orbitals:

$$E_{\mu\nu}^{ij'} = \frac{\langle \mathbf{R}_{ji}, \mathbf{n}(\nu_j) \rangle}{\|R_{ji}\|} V_{\mu\nu}^\sigma = E_{\nu\mu}^{ji'}, \quad (3.45)$$

$$E_{\nu\mu}^{ij'} = -\frac{\langle \mathbf{R}_{ji}, \mathbf{n}(\nu_i) \rangle}{\|R_{ji}\|} V_{\mu\nu}^\sigma = E_{\mu\nu}^{ji'}. \quad (3.46)$$

This case is illustrated in Fig. 3.9 considering s - p_x overlaps.

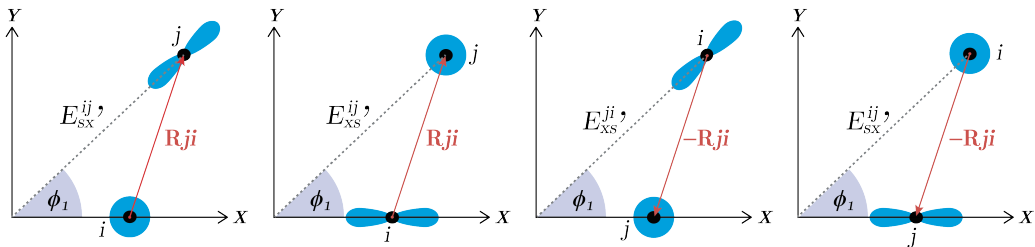


Figure 3.9: Interpretation 1 of atomic orbital orientation with no corrections.

The drawback with Interpretation 1 is due to the change in magnitude between atoms in $(\mathcal{M}, \mathcal{A})$ when either the position label or the orbital label are interchanged once (e.g. $E_{\mu\nu}^{ij} \neq E_{\nu\mu}^{ij}$ and $E_{\mu\nu}^{ij} \neq E_{\mu\nu}^{ji}$). The problem arises because Eqs. (3.45)- to (3.46) generate a change in angle when one of the labels of the matrix elements is changed. This angle is introduced by the parametrization $\mathbf{n}(\nu_{i,j})$ of the p orbital, which indicates that a change in the orbital orientation produces a change in the magnitude of the interaction between atomic orbitals. However, this observation cannot be true as the orbital overlaps must be independent of the reference system and thus cannot depend on the observer. Also, this interpretation break up inversion symmetry for overlaps with atoms in $(\mathcal{M}, \mathcal{A})$ and thus violates time reversal. It must be emphasized that this complication only arises for atoms in $(\mathcal{M}, \mathcal{A})$, while the other overlaps conserve the magnitude of Slater-Koster overlaps due to: (1) distance conservation, that is $\mathbf{R}_i = \mathbf{R}_j$ for atoms in either \mathcal{I} or \mathcal{A} (see Eqs. 3.29 to 3.37) and; (2) angle conservation, specifically $\Phi_i = \Phi_j$ which occur for atoms in $(\mathcal{I}, \mathcal{M})$ (see Eqs. 3.38 to 3.41).

As a consequence, another interpretation must be used in order to conserve the aforementioned symmetries. In that sense, Interpretation 2 consider the same parametrization given in Eqs. (3.45) to (3.46) but the matrix elements that appear in the hamiltonian do not rotate with respect to a interchange in label. That is, all the overlaps involving the same orbitals in the same atoms depend only in one angle given by $\mathbf{n}(\nu_j)$. Then, the correction to the matrix overlaps is done by conserving the same angle of the parametrization as:

$$E_{\mu\nu}^{ij} = \frac{\langle \mathbf{R}_{ji}, \mathbf{n}(\nu_j) \rangle}{\|R_{ji}\|} V_{\mu\nu}^\sigma = E_{\nu\mu}^{ji}, \quad (3.47)$$

$$E_{\nu\mu}^{ij} = -E_{\mu\nu}^{ij} = E_{\mu\nu}^{ji}. \quad (3.48)$$

Again, this another case is illustrated in Fig. 3.10 considering s - p_x overlaps.

Therefore, Eqs. (3.47) to (3.48) implies the same symmetries found in Eqs. (3.29) to (3.37) and thus this prescription can be extended to be applicable for atoms in $(\mathcal{M}, \mathcal{A})$ (in addition to atoms in \mathcal{I} and \mathcal{A}).

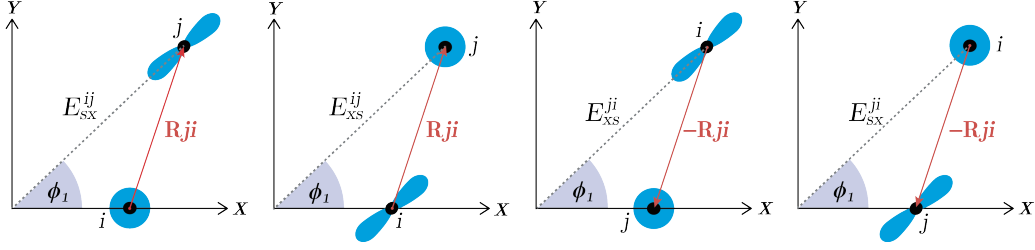


Figure 3.10: Interpretation 2 of atomic orbital orientation with corrections.

Finally, it is important to note that Interpretation 1 and 2 describe the same rotating system. The only problem that arose was with respect the conservation of angular momentum. The problem reduced to specify correctly the terms $E_{\mu\nu}^{ij}$, $E_{\nu\mu}^{ij}$, $E_{\mu\nu}^{ji}$ and $E_{\nu\mu}^{ji}$ so they conserve the angular momentum. In fact, this step only checks that the symmetries in the system are conserved, and as it will be seen, only one kinetic term (e.g $E_{\mu\nu}^{ij}$) is required to describe the helicene system.

3.4 Effective hamiltonian

The total hamiltonian of the helicene including perturbation effects can be written in the form given by Eq. (2.3). In this case, the helicene hamiltonian can be grouped following Eq. (2.29) and the procedure described in the Methodology section 1.4:

$$H = \begin{pmatrix} H_{\sigma} & T \\ T^{\dagger} & H_{\pi} \end{pmatrix}, \quad (3.49)$$

where H_{σ} and H_{π} are the structural hamiltonians (containing the σ - and π - bonding) and the T matrices includes the connection between H_{σ} and H_{π} spaces.

In general, the hamiltonian can be expanded in the basis of atomic orbitals, contemplating all the orbital interactions at nearest neighbours as:

$$\begin{array}{c}
|p_z\rangle_i \quad |p_z\rangle_j \quad |s\rangle_i \quad |p_x\rangle_i \quad |p_y\rangle_i \quad |s\rangle_j \quad |p_x\rangle_j \quad |p_y\rangle_j \\
\begin{array}{c}
|p_z\rangle_i \\
|p_z\rangle_j \\
|s\rangle_i \\
|p_x\rangle_i \\
|p_y\rangle_i \\
|s\rangle_j \\
|p_x\rangle_j \\
|p_y\rangle_j
\end{array}
\left(\begin{array}{c|c}
H_\pi & T \\
\hline
T^\dagger & H_\sigma
\end{array} \right)
\end{array} \quad (3.50)$$

In this case, the subspace H_π contains the unperturbed p_z orbitals having in its diagonal the terms ϵ_p^π which are the bare energy of the p_z orbitals; and in the off-diagonal the overlap E_{zz}^{ij} .

$$H_\pi = \begin{pmatrix} \epsilon_p^\pi & E_{zz}^{ij} \\ E_{zz}^{ij} & \epsilon_p^\pi \end{pmatrix} \quad (3.51)$$

On the other hand, the H_σ submatrix contains the following energies in its diagonal: ϵ_p^π which define the site energy for the p_x and p_y bonded orbitals; ϵ_p^σ the site energy of the p_z orbital, and ϵ_s the energy of the s orbital. Meanwhile, the off-diagonal terms contain the coupling between these orbitals.

$$H_\sigma = \begin{pmatrix}
\epsilon_s & 0 & 0 & E_{ss}^{ij} & E_{sx}^{ij} & E_{sy}^{ij} \\
0 & \epsilon_p^\sigma & -i(\mathbf{s}_z \xi_p + \mu_p) & E_{xs}^{ij} & E_{xx}^{ij} & E_{xy}^{ij} \\
0 & i(\mathbf{s}_z \xi_p + \mu_p) & \epsilon_p^\sigma & E_{ys}^{ij} & E_{yx}^{ij} & E_{yy}^{ij} \\
E_{ss}^{ij} & E_{xs}^{ij} & E_{ys}^{ij} & \epsilon_p^\sigma & 0 & 0 \\
E_{sx}^{ij} & E_{xx}^{ij} & E_{sx}^{ij} & 0 & \epsilon_p^\sigma & -i(\mathbf{s}_z \xi_p + \mu_p) \\
E_{sy}^{ij} & E_{xy}^{ij} & E_{yy}^{ij} & 0 & i(\mathbf{s}_z \xi_p + \mu_p) & \epsilon_p^\sigma
\end{pmatrix} \quad (3.52)$$

As it can be noticed, the SOC and Zeeman interactions couple the π electrons to the on-site p_x and p_y orbitals.

Finally, the T subspace contains the intrinsic SOC, the Stark couplings, and the overlaps between the orbitals p_z with the s , p_x , p_y and p_z orbitals.

$$T = \begin{pmatrix} \xi_{sp} & -i\mathbf{s}_y\xi_p & i\mathbf{s}_x\xi_p & E_{zs}^{ij} & E_{zx}^{ij} & E_{zy}^{ij} \\ E_{sz}^{ij} & E_{xz}^{ij} & E_{yz}^{ij} & \xi_{sp} & -i\mathbf{s}_y\xi_p & i\mathbf{s}_x\xi_p \end{pmatrix} \quad (3.53)$$

The problem of computing $TH_\sigma^{-1}T^\dagger$ relies in its computational cost and the many number of variables to process in reducing the original 8×8 site and orbital space into just a 2×2 decimated space. However, this problem can be overcome by eliminating variables which in principle do not participate in the electronic transport such as those appearing in the σ -bonding and also variables which do not appear at first order with respect the Feynmann paths. Then, under this premise, the matrix elements that can be neglected are:

$$E_{xx}^{ij}, E_{yy}^{ij}, E_{xy}^{ij}, E_{yx}^{ij} = 0 \quad (3.54)$$

In fact, these terms contribute to the electronic transport but they appear at higher orders in the Feynman path. Even if the paths that include the terms in Eq. (3.54) are possible, they are unlikely to occur, and so they can be neglected. Additionally, it can be used the symmetry relations for nearest neighbours in \mathcal{I} , \mathcal{A} , and $(\mathcal{M}, \mathcal{A})$:

$$E_{sx}^{ij} = E_{xs}^{ij} = E_{xs}^{ji} \quad (3.55)$$

$$E_{sy}^{ij} = -E_{ys}^{ij} = E_{ys}^{ji} \quad (3.56)$$

$$E_{sz}^{ij} = -E_{zs}^{ij} = E_{zs}^{ji} \quad (3.57)$$

$$E_{xy}^{ij} = -E_{yx}^{ij} = E_{yx}^{ji} \quad (3.58)$$

$$E_{xz}^{ij} = -E_{zx}^{ij} = E_{zx}^{ji} \quad (3.59)$$

$$E_{yz}^{ij} = E_{zy}^{ij} = E_{zy}^{ji}, \quad (3.60)$$

and the symmetry relations for nearest neighbours in $(\mathcal{I}, \mathcal{M})$ presented in Eqs. (3.38) to (3.41).

3.5 Magnitude of the interactions

In this section, the magnitude of the kinetic, spin-orbit, Rashba and Zeeman interactions are computed using the expressions obtained from the matrix decimation. All these calculations were preformed using the computer algebra software Mathematica.

3.5.1 Kinetic energy hamiltonian

The kinetic hamiltonian arises only due to the Slater-Koster overlaps between p_z orbitals. It is important to note that no further correction to the kinetic energy from the decimation procedure is considered. Thus, the kinetic hamiltonian can be written as:

$$\mathbf{H}_K = \sum_k t^k \sum_{(i,j)} a_i^\dagger a_j = \sum_k \sum_{(i,j)} E_{zz}^{ij} a_i^\dagger a_j, \quad (3.61)$$

where t^k indicates the hoppings between nearest-neighbor sites in $\alpha = \mathcal{I}, \mathcal{A}, (\mathcal{I}, \mathcal{M})$ and $(\mathcal{M}, \mathcal{A})$. Namely, these couplings arise between: two atoms in the inner helix or in \mathcal{I} ; two atoms in the outer helix or in \mathcal{A} ; one atom in the inner helix and one atom in the middle helix, or atoms in $(\mathcal{I}, \mathcal{M})$ and; one atom in the middle helix and one atom in the outer helix, or atoms in $(\mathcal{I}, \mathcal{M})$ (refer to Fig. 3.2). Thus, there are four kinetic coupling terms (e.g $t^{\mathcal{I}}, t^{\mathcal{A}}, t^{\mathcal{I}, \mathcal{M}}, t^{\mathcal{M}, \mathcal{A}}$) which correspond to the four inequivalent atoms in helicene. It should be noted that the interaction terms between sites on the same helix are \mathcal{I} and \mathcal{A} while $(\mathcal{I}, \mathcal{M})$ and $(\mathcal{M}, \mathcal{A})$ denote couplings between sites on different helices.

Then, all the kinetic couplings can be evaluate explicitly as:

$$t^{\mathcal{I}} = \frac{b^2 \phi_0 (V_{zz}^\sigma - V_{zz}^\pi)}{8\pi^2 a_0^2 [1 - \cos(\phi_0)] + b^2 \phi_0^2} = -1.806 \text{ eV} \quad (3.62)$$

$$t^{\mathcal{A}} = \frac{b^2 \phi_2 (V_{zz}^\sigma - V_{zz}^\pi)}{8\pi^2 a_1^2 [1 - \cos(\phi_2)] + b^2 \phi_2^2} = -3.191 \text{ eV} \quad (3.63)$$

$$t^{\mathcal{I}, \mathcal{M}} = V_{zz}^\pi = -3.440 \text{ eV} \quad (3.64)$$

$$t^{\mathcal{M}, \mathcal{A}} = \frac{b^2 \phi_1 (V_{zz}^\sigma - V_{zz}^\pi)}{4\pi^2 [4a_0^2 + a_1^2 - 4a_0 a_1 \cos(\phi_1)] + b^2 \phi_1^2} = -3.247 \text{ eV} \quad (3.65)$$

The values obtained for the kinetic terms have the same magnitude as the ones reported by Geyer et. al [19], which corroborates that the prescription used for Slater-Koster elements is correct. Additionally, these terms are two magnitude order higher than similar models obtained from DNA (e.g. $E_{zz}^{ij(\text{DNA})} \sim -10$ meV) [17]. This is because the Slater-Koster elements E_{zz}^{ij} are inversely proportional to the atom distance square $\|R_{ji}\|^2$. The square of the atomic distance for the helicene is $\|R_{ji}^H\|^2 = 1.4$ Å while for DNA is $\|R_{ji}^{\text{DNA}}\|^2 = 23.7$ Å [17]. As higher the atomic separation is, the lower the magnitude Slater-Koster overlap will be. Thus, the kinetic term for the helicene will be higher than the term of the DNA (b-type) bases. Despite the fact that the same equations reported for DNA [17] were derived for helicenes, the extent as the atomic orbitals overlaps will be determined by geometrical factors.

3.5.2 Spin-orbit hamiltonian

The intrinsic SOC in carbon atoms allows spin flip processes between in-site p orbitals and its contribution between sites i and j is given by:

$$\mathbf{H}_{\text{SO}}^{ij} = i \sum_k \alpha_y^k \sum_{(i,j)} a_i^\dagger \eta_{ij} \mathbf{s}_y a_j, \quad (3.66)$$

where $\eta_{ij} = \text{sgn}(j - i)$ and α is the intrinsic SO vector whose magnitude is computed as:

$$\alpha_y = -\frac{2i\xi_p E_{xz}^{ij}(\epsilon_p^\pi - \epsilon_s^\sigma)}{(E_{sx}^{ij})^2 + (E_{sy}^{ij})^2 + (\epsilon_p^\pi - \epsilon_p^\sigma)(\epsilon_p^\pi - \epsilon_s^\sigma)}. \quad (3.67)$$

Considering the structural characteristics of the helicene, the estimated values for the SOC magnitudes in the y coordinate are $\alpha_y^{\mathcal{I}} = 1.83$ meV, $\alpha_y^{(\mathcal{M}, \mathcal{A})} = 1.70$ meV and $\alpha_y^{\mathcal{A}} = -0.25$ meV while the terms in the z direction are negligible as they appear at third order. The highest value of α_y is achieved for atomic overlaps in the inner helix \mathcal{I} , which again corroborates the claim that the spin processes are given primarily through the inner helix.

In contrast to the kinetic terms, the perturbation effects appear in combination with the site energy terms (e.g. ϵ_p^π , ϵ_p^σ and ϵ_s). Geyer et al. considered degenerate energies for σ bonds, that is $\epsilon_p^\sigma = \epsilon_s$. However, this is not necessarily true and it can be demonstrated in perturbation theory $\epsilon_s = -17.52$ eV and $\epsilon_p^\pi = -8.97$ eV, while from Hückel theory $\epsilon_p^\pi - \epsilon_s \approx 2.5$ eV [47]. The SOC values from Geyer et. al may also contain artifacts (due to the perturbative method used) which overestimate the real ones. Additionally, Geyer et al. did not show any hermiticity check in the expression in their approach, and as mentioned in this work, this may led to violations of physical laws. Regardless of this facts, our works shows similar values for the SOC magnitude as it can be seen from Table 3.2.

Table 3.2: Obtained SOC couplings and literature referential values.

SOC terms (meV)		
	This Work	Geyer et. al
$\alpha_y^{\mathcal{I}}$	1.83	3.05
$\alpha_y^{(\mathcal{M}, \mathcal{A})}$	1.70	3.13
$\alpha_y^{\mathcal{A}}$	0.25	0.48
$\alpha_x^{\mathcal{I}}$	-0.0076	-3.63
$\alpha_x^{(\mathcal{M}, \mathcal{A})}$	-0.0024	-0.00072
$\alpha_x^{\mathcal{A}}$	-0.0031	4.56

It can be observed that the values obtained for α_y in both researches are in the order of meV, having the same order than that of the intrinsic SOC of carbon. This implies a connection between chirality and the intrinsic SOC, as the value of the latter indicates that the chirality must be nonzero [17]. Because the α_y contribution to the overall SOC is directly proportional to the helical pitch (given by E_{zx}^{ij}), this term would be absent in planar geometries such as graphene. On the contrary, the same term will present in helical structures such as DNA [17], carbon nanotubes [52], and of course helicenes. Thus, the

helical structure is crucial to produce non-zero SOC couplings.

3.5.3 Rashba hamiltonian

The Rashba coupling describes the splitting of energy levels as a result of SOC in the presence of an external field [54], which cause the mixing of α and π bands. The Rashba term arises naturally from the decimation procedure, and its contribution between sites i and j is given by

$$\mathbf{H}_{\text{SOC}}^{ij} = i \sum_k \lambda_y^k \sum_{(i,j)} a_i^\dagger \eta_{ij} \mathbf{s}_y a_j, \quad (3.68)$$

where λ_y is the magnitude of the Rashba coupling and it is computed as:

$$\lambda_y = \frac{2i\xi_p \xi_{sp} E_{sy}^{ij}}{(E_{sx}^{ij})^2 + (E_{sy}^{ij})^2 + (\epsilon_p^\pi - \epsilon_p^\sigma)(\epsilon_p^\pi - \epsilon_s^\sigma)}. \quad (3.69)$$

The estimated values for the Rashba contribution, corresponding to an electric magnitude $\xi_{sp} = 10.5$ eV, are $\lambda_y^{\mathcal{I}} = -20.08$ meV, $\lambda_y^{(\mathcal{M}, \mathcal{A})} = -15.18$ meV and $\lambda_y^{\mathcal{A}} = -22.74$ meV.

It can be observed that λ_y is one order higher compared to the merely SOC σ_y magnitude. Despite the fact that the energy contribution of the SOC interaction is rather small compared to the Rashba coupling, the SOC effect importance is due to its property of symmetry breaking in the system. In that sense, the intrinsic SOC alone is too weak to account for the CISS effect, but in combination with an electric field applied along the molecule, it can induce a significant spin-dependent transmission [25]. If the electric field used here is considered to be intrinsic to the structure, for instance, as dipoles associated with the helicene (considering hydrogen bonding), then the Rashba term is perhaps the most important contribution to the electron spin interaction, and therefore the main contribution to the CISS effect.

3.5.4 Zeeman hamiltonian

The Zeeman contribution between sites i and j in the z direction is given by

$$\mathbf{H}_Z^{ij} = \sum_k \mu_z^k \sum_{(i,j)} a_i^\dagger \mathbf{s}_y a_j, \quad (3.70)$$

where μ_z is the magnitude of the Zeeman coupling aligned with B_z and it is defined as:

$$\begin{aligned} \mu_z = & - \frac{2\xi_p \mu_p E_{yz}^{ij} (\epsilon_p^\pi - \epsilon_s^\sigma) \mathbf{s}_y}{(\epsilon_p^\pi - \epsilon_p^\sigma) \left((E_{sx}^{ij})^2 + (E_{sy}^{ij})^2 + (\epsilon_p^\pi - \epsilon_p^\sigma)(\epsilon_p^\pi - \epsilon_s^\sigma) \right)} \\ & + \frac{2\xi_p \xi_{sp} \mu_p E_{sx}^{ij} \mathbf{s}_x}{(\epsilon_p^\pi - \epsilon_p^\sigma) \left((E_{sx}^{ij})^2 + (E_{sy}^{ij})^2 + (\epsilon_p^\pi - \epsilon_p^\sigma)(\epsilon_p^\pi - \epsilon_s^\sigma) \right)} \end{aligned} \quad (3.71)$$

Then, the values for the Zeeman contribution in the z direction, considering an external magnetic field of $B_z = 40 \mu\text{T}$, are $\mu_z^\mathcal{T} = 1.92 \times 10^{-8} \text{ meV}$, $\mu_z^{(\mathcal{M}, \mathcal{A})} = 3.97 \times 10^{-8} \text{ meV}$ and $\mu_z^\mathcal{A} = 1.86 \times 10^{-8} \text{ meV}$.

In the presence of an external magnetic field aligned in the z direction, it is obtained real components of the magnetic term proportional to \mathbf{s}_y and \mathbf{s}_x which causes the otherwise degenerate spin-up and spin-down states of an isolated electron to split apart. This is in agreement with the Zeeman effect in an atom where the energy levels of the atom are split into several components in the presence of an external magnetic field [41]. Additionally, it can be observed that μ_z only appears when is coupled with the already weak SOC term ξ_p . Because μ_z is a combination of the geomagnetic field in z direction B_z and the SOC term ξ_p , its magnitude becomes extremely low so its effects are negligible.

The Zeeman effect can also be computed along the transverse directions. That is, setting the magnetic field along the x and y directions. Similarly to the B_z field which causes orthogonal orbitals (e.g. p_x with p_y) to couple in plane (see Appendix D.), a B_x and B_y field will cause the orbital couple p_z - p_y and p_z - p_x , respectively. Then, decimating and obtaining the Zeeman hamiltonian for a magnetic field along the x direction, it is obtained:

$$\mathbf{H}_Z^{ij} = i \sum_k \mu_x^k \sum_{(i,j)} a_i^\dagger \eta_{ij} a_j \quad (3.72)$$

where μ_x is the magnitude of the Zeeman coupling aligned with B_x and is defined as:

$$\mu_x = -\frac{2i\xi_{sp}\mu_p E_{sy}^{ij}}{(E_{sx}^{ij})^2 + (E_{sy}^{ij})^2 + (\epsilon_p^\pi - \epsilon_p^\sigma)(\epsilon_p^\pi - \epsilon_s^\sigma)} \quad (3.73)$$

The values for the Zeeman contribution in the x direction are $\mu_x^{\mathcal{I}} = 1.34 \times 10^{-5}$ meV, $\mu_x^{(\mathcal{M}, \mathcal{A})} = 1.01 \times 10^{-5}$ meV and $\mu_x^{\mathcal{A}} = -2.08 \times 10^{-9}$ meV.

Meanwhile, the Zeeman hamiltonian for a magnetic field along the y direction is:

$$\mathbf{H}_Z^{ij} = i \sum_k \mu_y^k \sum_{(i,j)} a_i^\dagger \eta_{ij} a_j \quad (3.74)$$

where μ_y is the magnitude of the Zeeman coupling aligned with B_y and is defined as:

$$\mu_y = \frac{2i\mu_p E_{xz}^{ij}(\epsilon_p^\pi - \epsilon_s^\sigma)}{(E_{sx}^{ij})^2 + (E_{sy}^{ij})^2 + (\epsilon_p^\pi - \epsilon_p^\sigma)(\epsilon_p^\pi - \epsilon_s^\sigma)} \quad (3.75)$$

The values for the Zeeman contribution in the y direction are $\mu_y^{\mathcal{I}} = 2.76 \times 10^{-6}$ meV, $\mu_y^{(\mathcal{M}, \mathcal{A})} = 1.06 \times 10^{-7}$ meV and $\mu_y^{\mathcal{A}} = 1.56 \times 10^{-7}$ meV.

In this case, the magnitude of the magnetic fields in the x and y directions are set equal to the z field, that is $B_x = B_y = B_z$. In contrast to the Zeeman effect in the z direction, the fields in the x and y directions produce only imaginary component terms. In overall, the orientation of the helicene with respect to the external field is crucial for the magnitude and size of the Zeeman terms. Even using the same magnitude for the external field, the Zeeman couplings are far different in the x , y and z directions. Moreover, the magnitude of the Zeeman couplings ranges from $\times 10^{-5}$ meV to $\times 10^{-9}$ meV for different direction of the external magnetic field and also for different helix couplings (e.g. \mathcal{I} , $(\mathcal{M}, \mathcal{A})$ and \mathcal{A}). Up to date, there is no other known effect that may increase significantly the magnitude of the Zeeman couplings nor if there is any mechanism in which the relative difference of the Zeeman couplings (which is up to four orders of magnitude) becomes important, that is, a mechanism susceptible to these changes have not yet been described.

Thus, the limitation of this model relies in that the weak external magnetic field considered in this work do not produce any symmetry-breaking and thus it has an inappreciable contribution. Further works may require the implementation of other sources of magnetic fields such as induced magnetic dipoles related to the exchange interaction or electron–electron dipolar interaction. Even if these effects by themselves are weak, they can couple together to yield significant electron pathways, as is in the case of the Rashba coupling. Analyze these effects become fundamental to elucidate the prime interactions that lead to the CISS effect. A more complete approach may also require the use of a more complete base, such as the inclusion of d orbitals, which may lead to additional first order corrections.

CONCLUSIONS

In this work, spin interactions of helicenes were studied including the effects of electric fields, intrinsic SOC and external magnetic field. A minimal analytic tight-binding model was constructed to then describe the mobile electrons of the helical structure using the Slater-Koster Tight-Binding approach. A matrix decimation strategy from perturbative band folding was used to derive an effective Hamiltonian including the contribution of: (1) Kinetic energy, (2) Stark electric coupling, (3) intrinsic SOC, (4) Rashba-type coupling and (5) Zeeman external magnetic field coupling. It was obtained explicit analytical expressions in terms of geometric parameters as well as atomic orbital overlaps between nearest neighbor sites along each helix of the Helicenes.

The interaction effects cause that certain paths to be favored, which in turn produce that the p orbitals to be no longer degenerate. The favored paths can be used to approximate the effective interactions in the system which maintain the physics of the model while reduce unimportant variables. The decimation procedure takes advantage of this by neglecting Slater-Koster overlaps that do not contribute in the favored paths. Additionally, the Slater-Koster overlaps depend on the geometric parameters of a molecule, which give insights on the physical processes occurring in the system.

On the other hand, it was obtained analytical expression for the interaction effects, namely spin-orbit, Stark and Zeeman terms. It was found that the greatest SOC contribution comes from the term α_y and varies from 0.2 to 1.8 meV depending of the orbital couplings between helices in the system. In addition, the Rashba term yields a major contribution and its magnitude varies from 15 to 20 eV. On the contrary, the external magnetic field yield the lowest energy contributions with orders from 0.01 to 10 μeV depending on both the direction of the external field and the helix coupling.

The lack of SOC between atoms in $(\mathcal{I}, \mathcal{M})$ implies that spin-flip processes only occur along either the inner \mathcal{I} and outer \mathcal{A} helices. Moreover, the magnitude of σ_y derived from SOC is also great in \mathcal{I} than other helix couplings in helicene, which corroborates that spin processes have a preferential transmission through the helicene inner helix. This is also a reason why the Slater-Koster overlaps have the same form as the one derived from DNA [17, 23] systems having a similar helix atom/base distribution, as their electronic distribution is similar.

APPENDIX A

DERIVATION OF GENERAL OVERLAP EXPRESSION

First, it is important to define the inner (scalar) product. The inner product on the vector space V is a function $V \times V \rightarrow \mathbb{R}$ which associates each pair (\mathbf{x}, \mathbf{y}) of vectors in V with a real number $\langle \mathbf{x}, \mathbf{y} \rangle$ and satisfies the following conditions [55]:

$$\begin{aligned}\langle \mathbf{x}, \mathbf{x} \rangle &> 0 \text{ if } \mathbf{x} \neq \mathbf{0} \\ \langle \mathbf{x}, \mathbf{y} \rangle &= \langle \mathbf{y}, \mathbf{x} \rangle \\ \langle a\mathbf{x} + b\mathbf{y}, \mathbf{z} \rangle &= a \langle \mathbf{x}, \mathbf{z} \rangle + b \langle \mathbf{y}, \mathbf{z} \rangle\end{aligned}\tag{A.1}$$

where a and b are real numbers. It is important to note that the commonly used inner product in \mathbb{R}^n is denoted by $\mathbf{x} \cdot \mathbf{y}$ and expressed as [55]:

$$\mathbf{x} \cdot \mathbf{y} = x_1 y_1 + \dots + x_n y_n\tag{A.2}$$

where \mathbf{x} and \mathbf{y} are vectors with n components. Also, this definition satisfies the inner product conditions.

Then, we start from equation 3.2 and replace the projections 3.3 and 3.4. Based on these equations, there are two possible combination which are between p - p and s - p orbital overlaps. First, it is derived a general prescription to calculate $s - p$ overlaps

and then it is followed to obtain the p - p overlaps. As only geometrical considerations are taken into account to obtain the Slater-Koster overlaps, an s - p is equivalent to a p - s overlap as long as this terms are real numbers. Without loss of generalization, it is taken $\mathbf{n}(\mu_i) = \mathbf{n}(\mu_i)^\parallel = \mathbf{R}_{ij}/\|\mathbf{R}_{ij}\|$ so then:

$$H_{\mu\nu}^{ij} = \left\langle \mathbf{n}(\mu_i)^\parallel, \mathbf{n}(\nu_j)^\parallel \right\rangle V_{\mu\nu}^\sigma + \left\langle \mathbf{n}(\mu_i)^\perp, \mathbf{n}(\nu_j)^\perp \right\rangle V_{\mu\nu}^\pi = \left\langle \frac{\mathbf{R}_{ji}}{\|\mathbf{R}_{ji}\|}, \frac{\langle \mathbf{R}_{ij}, \mathbf{n}(\nu_j) \rangle}{\|\mathbf{R}_{ij}\|^2} \mathbf{R}_{ij} \right\rangle V_{\mu\nu}^\sigma \quad (\text{A.3})$$

By taking out the real numbers from the inner product, and redefining $\langle \mathbf{R}_{ji}, \mathbf{R}_{ji} \rangle = \|\mathbf{R}_{ji}\|^2$ it is obtained a general formula to compute $s - p$ overlaps:

$$H_{\mu\nu}^{ij} = \frac{\langle \mathbf{R}_{ij}, \mathbf{n}(\nu_j) \rangle}{\|\mathbf{R}_{ij}\|^3} \langle \mathbf{R}_{ji}, \mathbf{R}_{ij} \rangle V_{\mu\nu}^\sigma = \frac{\langle \mathbf{R}_{ij}, \mathbf{n}(\nu_j) \rangle}{\|\mathbf{R}_{ij}\|} V_{\mu\nu}^\sigma \quad (\text{A.4})$$

Next, for p - p overlaps, the replacement of the projections 3.3 and 3.4 led to the inner products:

$$H_{\mu\nu}^{ij} = \left\langle \frac{\langle \mathbf{R}_{ji}, \mathbf{n}(\mu_i) \rangle}{\|\mathbf{R}_{ji}\|^2} \mathbf{R}_{ji}, \frac{\langle \mathbf{R}_{ij}, \mathbf{n}(\nu_j) \rangle}{\|\mathbf{R}_{ij}\|^2} \mathbf{R}_{ij} \right\rangle V_{\mu\nu}^\sigma + \left\langle \mathbf{n}(\mu_i) - \frac{\langle \mathbf{R}_{ji}, \mathbf{n}(\mu_i) \rangle}{\|\mathbf{R}_{ji}\|^2} \mathbf{R}_{ji}, \mathbf{n}(\nu_j) - \frac{\langle \mathbf{R}_{ij}, \mathbf{n}(\nu_j) \rangle}{\|\mathbf{R}_{ij}\|^2} \mathbf{R}_{ij} \right\rangle V_{\mu\nu}^\pi \quad (\text{A.5})$$

Considering that $\mathbf{R}_{ji} = -\mathbf{R}_{ij}$ and $\|\mathbf{R}_{ji}\|^2 = \|\mathbf{R}_{ij}\|^2$, all interatomic distances can be written in terms of one parameter so that:

$$H_{\mu\nu}^{ij} = \left\langle \frac{\langle \mathbf{R}_{ji}, \mathbf{n}(\mu_i) \rangle}{\|\mathbf{R}_{ji}\|^2} \mathbf{R}_{ji}, \frac{\langle \mathbf{R}_{ji}, \mathbf{n}(\nu_j) \rangle}{\|\mathbf{R}_{ji}\|^2} \mathbf{R}_{ji} \right\rangle V_{\mu\nu}^\sigma + \left\langle \mathbf{n}(\mu_i) - \frac{\langle \mathbf{R}_{ji}, \mathbf{n}(\mu_i) \rangle}{\|\mathbf{R}_{ji}\|^2} \mathbf{R}_{ji}, \mathbf{n}(\nu_j) - \frac{\langle \mathbf{R}_{ji}, \mathbf{n}(\nu_j) \rangle}{\|\mathbf{R}_{ji}\|^2} \mathbf{R}_{ji} \right\rangle V_{\mu\nu}^\pi \quad (\text{A.6})$$

Using the distributive property of the inner product and noticing that real values can be taken out from the inner product

$$H_{\mu\nu}^{ij} = \left[\frac{\langle \mathbf{R}_{ji}, \mathbf{n}(\mu_i) \rangle}{\|\mathbf{R}_{ji}\|^2} \cdot \frac{\langle \mathbf{R}_{ji}, \mathbf{n}(\nu_j) \rangle}{\|\mathbf{R}_{ji}\|^2} \langle \mathbf{R}_{ji}, \mathbf{R}_{ji} \rangle \right] V_{\mu\nu}^\sigma + \left[\langle \mathbf{n}(\mu_i), \mathbf{n}(\nu_j) \rangle - \frac{\langle \mathbf{R}_{ji}, \mathbf{n}(\nu_j) \rangle}{\|\mathbf{R}_{ji}\|^2} \langle \mathbf{n}(\mu_i), \mathbf{R}_{ji} \rangle - \frac{\langle \mathbf{R}_{ji}, \mathbf{n}(\mu_i) \rangle}{\|\mathbf{R}_{ji}\|^2} \langle \mathbf{n}(\nu_j), \mathbf{R}_{ji} \rangle + \frac{\langle \mathbf{R}_{ji}, \mathbf{n}(\nu_j) \rangle}{\|\mathbf{R}_{ji}\|^2} \cdot \frac{\langle \mathbf{R}_{ji}, \mathbf{n}(\mu_i) \rangle}{\|\mathbf{R}_{ji}\|^2} \langle \mathbf{R}_{ji}, \mathbf{R}_{ji} \rangle \right] V_{\mu\nu}^\pi \quad (\text{A.7})$$

This expression can be further simplified by noticing that $\langle \mathbf{R}_{\mathbf{ji}}, \mathbf{R}_{\mathbf{ji}} \rangle = \|\mathbf{R}_{\mathbf{ji}}\|^2$ and by symmetry the terms $\langle \mathbf{n}(\mu_i), \mathbf{R}_{\mathbf{ji}} \rangle = \langle \mathbf{R}_{\mathbf{ji}}, \mathbf{n}(\mu_i) \rangle$ and $\langle \mathbf{n}(\nu_j), \mathbf{R}_{\mathbf{ji}} \rangle = \langle \mathbf{R}_{\mathbf{ji}}, \mathbf{n}(\nu_j) \rangle$ are equal. Hence, it is obtained:

$$H_{\mu\nu}^{ij} = \frac{\langle \mathbf{R}_{\mathbf{ji}}, \mathbf{n}(\mu_i) \rangle}{\|\mathbf{R}_{\mathbf{ji}}\|^2} \langle \mathbf{R}_{\mathbf{ji}}, \mathbf{n}(\nu_j) \rangle V_{\mu\nu}^\sigma + \left[\langle \mathbf{n}(\mu_i), \mathbf{n}(\nu_j) \rangle - \frac{\langle \mathbf{R}_{\mathbf{ji}}, \mathbf{n}(\nu_j) \rangle}{\|\mathbf{R}_{\mathbf{ji}}\|^2} \langle \mathbf{R}_{\mathbf{ji}}, \mathbf{n}(\mu_i) \rangle \right. \\ \left. - \frac{\langle \mathbf{R}_{\mathbf{ji}}, \mathbf{n}(\mu_i) \rangle}{\|\mathbf{R}_{\mathbf{ji}}\|^2} \langle \mathbf{R}_{\mathbf{ji}}, \mathbf{n}(\nu_j) \rangle + \frac{\langle \mathbf{R}_{\mathbf{ji}}, \mathbf{n}(\nu_j) \rangle}{\|\mathbf{R}_{\mathbf{ji}}\|^2} \langle \mathbf{R}_{\mathbf{ji}}, \mathbf{n}(\mu_i) \rangle \right] V_{\mu\nu}^\pi \quad (\text{A.8})$$

Finally, the last equation can be simplified and rearranged to yield the known result for p - p overlaps:

$$H_{\mu\nu}^{ij} = \frac{\langle \mathbf{R}_{\mathbf{ji}}, \mathbf{n}(\mu_i) \rangle}{\|\mathbf{R}_{\mathbf{ji}}\|^2} \langle \mathbf{R}_{\mathbf{ji}}, \mathbf{n}(\nu_j) \rangle V_{\mu\nu}^\sigma + \left[\langle \mathbf{n}(\mu_i), \mathbf{n}(\nu_j) \rangle - \frac{\langle \mathbf{R}_{\mathbf{ji}}, \mathbf{n}(\mu_i) \rangle}{\|\mathbf{R}_{\mathbf{ji}}\|^2} \langle \mathbf{R}_{\mathbf{ji}}, \mathbf{n}(\nu_j) \rangle \right] V_{\mu\nu}^\pi \quad (\text{A.9})$$

The results for the s - p and p - p overlaps can be summarized in the equations:

$$H_{\mu\nu}^{ij} = \langle \mathbf{n}(\mu_i), \mathbf{n}(\nu_j) \rangle V_{\mu\nu}^\pi + \frac{\langle \mathbf{R}_{\mathbf{ji}}, \mathbf{n}(\mu_i) \rangle}{\|\mathbf{R}_{\mathbf{ji}}\|^2} \langle \mathbf{R}_{\mathbf{ji}}, \mathbf{n}(\nu_j) \rangle (V_{\mu\nu}^\sigma - V_{\mu\nu}^\pi) \quad (\text{A.10})$$

which applies for $\mu, \nu \in (x, y, z)$ and

$$H_{\mu\nu}^{ij} = \frac{\langle \mathbf{R}_{\mathbf{ij}}, \mathbf{n}(\nu_j) \rangle}{\|\mathbf{R}_{\mathbf{ij}}\|} V_{\mu\nu}^\sigma \quad (\text{A.11})$$

which works for μ and $\nu \in (x, y, z)$. These equations are the same present in Eq. (3.6).

APPENDIX B

DERIVATION OF THE SPIN-ORBIT TERMS

The SOC Hamiltonian is defined as:

$$\mathbf{H}_{\text{SOC}} = \lambda \mathbf{L} \cdot \mathbf{S} \quad (\text{B.1})$$

By noticing that $\mathbf{J}^2 = (\mathbf{L} + \mathbf{S})^2 = (\mathbf{L}^2 + \mathbf{S}^2 + 2\mathbf{LS})$, the SOC Hamiltonian can be rewritten as:

$$\mathbf{H}_{\text{SOC}} = \frac{\lambda}{2} (\mathbf{L}^2 + \mathbf{S}^2 + 2\mathbf{LS}) \quad (\text{B.2})$$

Then, the SOC matrix elements can be computed using the couple basis given in Eq. (2.21) as follows:

$$E_{\text{SOC}} = \frac{\lambda}{2} \langle J, m_j | \mathbf{L}^2 + \mathbf{S}^2 + 2\mathbf{LS} | J, m_j \rangle \quad (\text{B.3})$$

For instance, to calculate the couplings between p_x and p_y orbitals through SOC. The non-vanishing overlaps are given by orbitals having the same spin, and written combination of coupled states $|J, m_j\rangle$, they are:

$$\begin{aligned} \langle p_x \uparrow | &= \left\langle \frac{3}{2}, \frac{3}{2} \right| - \sqrt{\frac{1}{3}} \left\langle \frac{3}{2}, \frac{1}{2} \right| + \sqrt{\frac{2}{3}} \left\langle \frac{1}{2}, -\frac{1}{2} \right| \\ |p_y \uparrow \rangle &= \left\langle \frac{3}{2}, \frac{3}{2} \right| + \sqrt{\frac{1}{3}} \left\langle \frac{3}{2}, \frac{1}{2} \right| - \sqrt{\frac{2}{3}} \left\langle \frac{1}{2}, -\frac{1}{2} \right| \end{aligned} \quad (\text{B.4})$$

It is important to note that the p orbitals written in the form $|J, m_j\rangle$ have implicit the quantum states $|l, m_l\rangle$ and $|s, m_s\rangle$. To apply any of the operators of the CSCO given in Eq. (2.16), one have to take into account that the system is modelled by mobile electrons (spin 1/2 system) constrained to s and p orbitals. That is, $s = 1/2$ and $l = 1$ for p orbitals, which applies for every state in the Helicene. Using the eigenvalues given in Eq. (2.17), it is easy to find that:

$$\begin{aligned}\mathbf{S}^2 \left| \frac{1}{2}, m_s \right\rangle &= \frac{3}{4} \hbar^2 \left| \frac{1}{2}, m_s \right\rangle \\ \mathbf{L}^2 |1, m_l\rangle &= \hbar^2 |1, m_l\rangle\end{aligned}\tag{B.5}$$

where $m_s = 1/2, -1/2$ while $m_l = -1, 0, 1$. Lastly, consider that the only eigenvalue possible for the total angular momentum are:

$$\begin{aligned}\mathbf{J}^2 \left| \frac{3}{2}, m_j \right\rangle &= \frac{15}{4} \hbar^2 \left| \frac{3}{2}, m_j \right\rangle \\ \mathbf{J}^2 \left| \frac{3}{2}, m_j \right\rangle &= \frac{15}{4} \hbar^2 \left| \frac{3}{2}, m_j \right\rangle\end{aligned}\tag{B.6}$$

Applying the prescription given in Eq.B.3 and considering the eigenvalues from Eqs. B.5 and B.6, it can be obtained:

$$\begin{aligned}E_{\text{SOC}} &= \langle p_x \uparrow | \mathbf{L}^2 + \mathbf{S}^2 + 2\mathbf{LS} | p_y \uparrow \rangle \\ &= -\frac{\lambda}{2} \left[\left\langle \frac{3}{2}, \frac{3}{2} \right| - \sqrt{\frac{1}{3}} \left\langle \frac{3}{2}, \frac{1}{2} \right| + \sqrt{\frac{2}{3}} \left\langle \frac{1}{2}, -\frac{1}{2} \right| \right] \left(\frac{1}{2} (\mathbf{J}^2 - \mathbf{L}^2 - \mathbf{S}^2) \right) \\ &\quad i \left[\left\langle \frac{3}{2}, \frac{3}{2} \right| + \sqrt{\frac{1}{3}} \left\langle \frac{3}{2}, \frac{1}{2} \right| - \sqrt{\frac{2}{3}} \left\langle \frac{1}{2}, -\frac{1}{2} \right| \right] \\ &= -\frac{\lambda}{4} \hbar^2 \left[\frac{15}{4} - 2 - \frac{3}{4} - \frac{1}{3} \left(\frac{15}{4} - 2 - \frac{3}{4} \right) - \frac{2}{3} \left(\frac{3}{4} - 2 - \frac{3}{4} \right) \right] = -i \frac{\lambda}{2} \hbar^2\end{aligned}\tag{B.7}$$

APPENDIX C

DERIVATION OF THE STARK TERM

The Stark Hamiltonian in the z direction can be written in spherical coordinates in the rotating basis as:

$$\mathbf{H}_S = -eE_z \hat{z} = -eE_z r \cos(\theta) \quad (\text{C.1})$$

In this case, due to s orbital spherical symmetry, is convenient to treat the overlaps with the spherical harmonics functions instead of the so far used bra-ket formulation. Then, the atomic orbitals in spherical coordinates are described by the hydrogenic wavefunctions [47]:

$$\begin{aligned} \psi_s = (\mathbf{r}) = \langle \mathbf{r} | s \rangle &= \frac{1}{\sqrt{32\pi a_0^3}} e^{-r/2a_0} \left(2 - \frac{r}{a_0} \right) \\ \psi_x = (\mathbf{r}) = \langle \mathbf{r} | p_x \rangle &= \frac{1}{\sqrt{64\pi a_0^3}} e^{-r/2a_0} \frac{r}{a_0} \sin(\theta) \cos(\phi) \\ \psi_y = (\mathbf{r}) = \langle \mathbf{r} | p_y \rangle &= -\frac{1}{\sqrt{64\pi a_0^3}} e^{-r/2a_0} \frac{r}{a_0} \sin(\theta) \sin(\phi) \\ \psi_z = (\mathbf{r}) = \langle \mathbf{r} | p_z \rangle &= \frac{1}{\sqrt{32\pi a_0^3}} e^{-r/2a_0} \frac{r}{a_0} \cos(\theta) \end{aligned} \quad (\text{C.2})$$

where a_0 is the Bohr radius and the wavefunctions ψ_s and $\psi_{x,y,z}$ are referred to the atomic orbitals $2s$ and $2p_{x,y,z}$ respectively. Additionally, the hydrogenic wavefunction

can be separated into a radial $R_n(\mathbf{r})$ and angular $Y_{lm}(\theta, \phi)$ part, with Y_{lm} the spherical harmonic function. Moreover, the spherical harmonics can be regarded as a unitary transformation from the angular momentum to the angular component representation [39] as follows $Y_{lm}(\theta, \phi) = \langle \theta\phi | lm \rangle$.

$$\xi_{sp} = \langle \psi_s | H_S | \psi_z \rangle = -eE_z \langle \psi_s | r \cos(\theta) | \psi_z \rangle \quad (\text{C.3})$$

Then, by replacing the hydrogenic wavefunctions it is obtained:

$$\xi_{sp} = -\frac{eE_z}{32\pi a_0^3} \int_{\Omega} e^{-r/a_0} \frac{r^2}{a_0} \left(2 - \frac{r}{a_0}\right) \cos(\theta) dV \quad (\text{C.4})$$

where Ω is the region delimited by $r \in [0, \infty)$, $\theta \in [0, \pi]$, and $\phi \in [0, 2\pi)$ while the differential volume element in spherical coordinates is $dV = r^2 \sin(\theta) dr d\theta d\phi$. Therefore, the angular and radial components can be solved independently over the space integration region. By rearranging some terms, it is obtained:

$$\xi_{sp} = -\frac{eE_z}{32\pi} \int_0^{2\pi} \int_0^\pi \int_0^\infty e^{-r/a_0} \frac{r^4}{a_0^4} \left(2 - \frac{r}{a_0}\right) \cos^2(\theta) \sin(\theta) d\phi d\theta dr \quad (\text{C.5})$$

Working out the angular part it is obtained:

$$\int_0^{2\pi} d\phi \int_0^\pi \cos^2(\theta) \sin(\theta) d\theta = -2\pi \left. \frac{\cos^3(\theta)}{3} \right|_0^\pi = \frac{4\pi}{3} \quad (\text{C.6})$$

While for the radial part, it is made the change of variable $t = r/a_0$ so that $dt = dr/a_0$

$$\int_0^\infty e^{-r/a_0} \frac{r^4}{a_0^4} \left(2 - \frac{r}{a_0}\right) dr = a_0 \int_0^\infty e^{-t} (2t^4 - t^5) dt \quad (\text{C.7})$$

The improper integral can be evaluated using the Gamma function property:

$$\Gamma(z+1) = \int_0^\infty t^z e^{-t} dt = z! \quad (\text{C.8})$$

Thus, the radial integral becomes

$$a_0 \int_0^\infty e^{-t} (2t^4 - t^5) dt = a_0 (2 \cdot 4! - 5!) = -72a_0 \quad (\text{C.9})$$

By joining all the results, the Stark term can be written in the form:

$$\xi_{sp} = 3ea_0 E_z \quad (\text{C.10})$$

APPENDIX D

DERIVATION OF THE ZEEMAN TERMS

The Zeeman Hamiltonian is given by:

$$H_Z = \frac{e}{2m} (\mathbf{L} + 2\mathbf{S}) \cdot \mathbf{B} = \frac{e}{2m} (\mathbf{J} + \mathbf{S}) \cdot \mathbf{B} \quad (\text{D.1})$$

where we used the fact that $\hat{J} = \hat{L} + \hat{S}$. Because we are considering only a magnetic field in the z direction so that $\mathbf{B} = B_z \hat{e}_z$, the only terms remaining are the ones in the z direction:

$$\mathbf{H}_Z = \frac{eB_z}{2m} (J_z + S_z) \quad (\text{D.2})$$

To emulate the magnetic field of the Earth, the analysis of the external magnetic effects is restricted to the weak-field limit. Then, it can be used the SOC coupled basis to represent the p orbitals in the form $|j, m_j\rangle$ as given in Eq. (2.10). Then, the matrix elements can be computed using the operator:

$$\mathbf{H}_Z = \frac{eB_z}{2m} \langle j, m_j | J_z + S_z | j, m_j \rangle \quad (\text{D.3})$$

Using the projection lemma, S_z can be expressed in terms of \hat{J}_z , \hat{L}_z and \hat{S}_z .

$$S_z = \frac{(S_z \cdot J_z) J_z}{J_z^2} \quad (\text{D.4})$$

By noticing that $2S_z \cdot J_z = J_z^2 - L_z^2 + S_z^2$ and using the \hat{S}_z projection, the magnetic contribution to the total Hamiltonian can be computed as follows.

$$\begin{aligned} E_Z &= \frac{eB_z}{2mc} \left\langle J, m_j \left| \hat{J}_z + \frac{1}{2} \frac{(J_z^2 - L_z^2 + S_z^2) J_z}{J_z^2} \right| J, m_j \right\rangle \\ &= \frac{eB_z}{2mc} \left[\langle J, m_j | J_z | J, m_j \rangle \left(1 + \left\langle J, m_j \left| \frac{J_z^2 - L_z^2 + S_z^2}{\hat{J}_z^2} \right| J, m_j \right\rangle \right) \right] \end{aligned} \quad (D.5)$$

Then, the p orbitals can be expressed as a linear combination of coupled states. For instance, consider the external magnetic coupling $\langle p_x | \mathbf{H}_Z | p_y \rangle$. The non-vanishing terms occur when both orbitals have the same spin whose magnitude, according to Eq. (B.4). Then, applying the Zeeman operator and summing algebraically, it is obtained

$$E_Z = -\frac{eB_z}{4m} \left[2\hbar \left(1 + \frac{1}{2} \left[\frac{\frac{5}{2} - \frac{5}{6} + \frac{1}{3}}{2} \right] \right) \right] = -\frac{3}{4} \frac{eB_z \hbar}{mc} i = -\frac{3}{2} \mu_B B_z i \equiv -\mu_p i \quad (D.6)$$

Which finally yield the result:

$$E_Z = -\mu_p i \quad (D.7)$$

APPENDIX E

MODEL PARAMETERS AND ESTIMATED OVERLAPS

The geometric parameters used to model the helicene are given in Table E.1.

Table E.1: Helicene geometric parameters

Distances (Å)	Radii (Å)	Angles (rad)
$a_0 = 1.4$	$r_0 = a_0 = 1.4$	$\phi_0 = \frac{\pi}{3}$
$b = 3.6$	$r_1 = 2a_0 = 2.8$	$\phi_1 = \frac{191\pi}{1800}$
	$r_2 = \sqrt{7}a_0 = 3.7$	$\phi_2 = \frac{109\pi}{900}$

On the other hand, based on Geyer et al. [19], the values of Slater-Koster parameters are summarized in Table E.2. The Slater-Koster parameters V_{pp} and V_{sp} can be replaced for specific combinations of s and p orbitals with the correct bonding-type (e.g $V_{pp}^\pi = V_{xy}^\pi = V_{zz}^\pi$) as long as they satisfy the rule $V_{l,l'} = (-1)^{l+l'} V_{l',l}$.

Table E.2: Slater-Koster parameters for helicenes

$V_{ss} = -7.92$ eV	$V_{pp}^\sigma = 7.09$ eV
$V_{sp}^\sigma = 8.08$ eV	$V_{pp}^\pi = 3.44$ eV

Still on the subject, the self-energies of the p and s orbitals, as well as the magnitude of the electric and magnetic interactions are given in Table E.3.

Table E.3: Atomic site self energy and magnitude of interaction effects.

Self Energy (eV)	Interaction Magnitude (eV)
$\epsilon_s = -17.52$	$\xi_p = 0.006$
$\epsilon_p^\sigma = -11.47$	$\xi_{sp} = 10.5$
$\epsilon_p^\pi = -8.97$	$\mu_p = 4 \times 10^{-9}$

Based on the values reported in Tables E.1-E.3, the Slater-Koster overlaps can be computed for the different couplings between helices in helicene. For convenience, these values are divided in three groups. First, overlaps between atomic orbitals in \mathcal{I} helix are presented in Table E.4.

Table E.4: Slater-Koster overlaps in \mathcal{I} helix

$E_{sx}^{ij} = 4.04 \text{ eV}$	$E_{xy}^{ij} = 1.40 \text{ eV}$
$E_{sy}^{ij} = 7.00 \text{ eV}$	$E_{xz}^{ij} = -0.78 \text{ eV}$
$E_{sz}^{ij} = 3.46 \text{ eV}$	$E_{yz}^{ij} = 1.35 \text{ eV}$

Second, overlaps between atomic orbitals in $(\mathcal{M}, \mathcal{A})$ helices are shown in Table E.5.

Table E.5: Slater-Koster overlaps $(\mathcal{M}, \mathcal{A})$

$E_{sx}^{ij} = 6.11 \text{ eV}$	$E_{xy}^{ij} = 2.32 \text{ eV}$
$E_{sy}^{ij} = 5.29 \text{ eV}$	$E_{xz}^{ij} = 0.25 \text{ eV}$
$E_{sz}^{ij} = 1.10 \text{ eV}$	$E_{yz}^{ij} = 0.43 \text{ eV}$

And third, overlaps between atomic orbitals in (\mathcal{A}) helix can be seen in Table E.6

Table E.6: Slater-Koster overlaps \mathcal{A}

$E_{sx}^{ij} = 1.53 \text{ eV}$	$E_{xy}^{ij} = 0.60 \text{ eV}$
$E_{sy}^{ij} = 7.94 \text{ eV}$	$E_{xz}^{ij} = -0.11 \text{ eV}$
$E_{sz}^{ij} = 1.26 \text{ eV}$	$E_{yz}^{ij} = 0.56 \text{ eV}$

BIBLIOGRAPHY

- [1] I. Žutić, J. Fabian, and S. Das Sarma, “Spintronics: Fundamentals and applications,” *Reviews of Modern Physics*, vol. 76, pp. 323–410, apr 2004.
- [2] S. Sanvito, “Molecular spintronics,” *Chem. Soc. Rev.*, vol. 40, no. 6, pp. 3336–3355, 2011.
- [3] S. D. Bader and S. S. P. Parkin, “Spintronics,” *Annual Review of Condensed Matter Physics*, vol. 1, no. 1, pp. 71–88, 2010.
- [4] Y. Xu, D. Awschalom, and J. Nitta, *Handbook of spintronics*. Springer Netherlands, 2016.
- [5] S. Bandyopadhyay and M. Cahay, *Introduction to spintronics*. CRC press, 2015.
- [6] H. Ohno, M. D. Stiles, and B. Dieny, “Spintronics,” *Proceedings of the IEEE. Institute of Electrical and Electronics Engineers*, vol. 104, pp. 1782–1786, oct 2016.
- [7] J. Wang, H. Meng, and J.-P. Wang, “Programmable spintronics logic device based on a magnetic tunnel junction element,” *Journal of Applied Physics*, vol. 97, no. 10, p. 10D509, 2005.

- [8] W. Naber and W. Wiel, “TOPICAL REVIEW: Organic spintronics,” *Journal of Physics D Applied Physics*, vol. 40, p. 205, 2007.
- [9] M. N. Baibich, J. M. Broto, A. Fert, F. N. Van Dau, F. Petroff, P. Etienne, G. Creuzet, A. Friederich, and J. Chazelas, “Giant Magnetoresistance of (001)Fe/(001)Cr Magnetic Superlattices,” *Phys. Rev. Lett.*, vol. 61, pp. 2472–2475, nov 1988.
- [10] G. Binasch, P. Grünberg, F. Saurenbach, and W. Zinn, “Enhanced magnetoresistance in layered magnetic structures with antiferromagnetic interlayer exchange,” *Phys. Rev. B*, vol. 39, pp. 4828–4830, mar 1989.
- [11] E. E. Fullerton and I. K. Schuller, “The 2007 Nobel Prize in Physics: magnetism and transport at the nanoscale,” *ACS nano*, vol. 1, no. 5, pp. 384–389, 2007.
- [12] K. Ray, S. P. Ananthavel, D. H. Waldeck, and R. Naaman, “Asymmetric scattering of polarized electrons by organized organic films of chiral molecules,” *Science (New York, N.Y.)*, vol. 283, pp. 814–816, feb 1999.
- [13] R. Naaman and D. H. Waldeck, “Spintronics and Chirality: Spin Selectivity in Electron Transport Through Chiral Molecules,” *Annual Review of Physical Chemistry*, vol. 66, pp. 263–281, apr 2015.
- [14] B. Göhler, V. Hamelbeck, T. Markus, M. Kettner, G. Hanne, Z. Vager, R. Naaman, and H. Zacharias, “Spin Selectivity in Electron Transmission Through Self-Assembled Monolayers of Double-Stranded DNA,” *Science (New York, N.Y.)*, vol. 331, pp. 894–897, 2011.
- [15] R. Naaman, Y. Paltiel, and D. H. Waldeck, “Chiral Molecules and the Spin Selectivity Effect,” *The Journal of Physical Chemistry Letters*, vol. 11, pp. 3660–3666, may 2020.
- [16] R. Naaman, Y. Paltiel, and D. H. Waldeck, “Chiral Induced Spin Selectivity Gives a New Twist on Spin-Control in Chemistry,” *Accounts of Chemical Research*, vol. 53, pp. 2659–2667, nov 2020.

- [17] S. Varela, V. Mujica, and E. Medina, “Effective spin-orbit couplings in an analytical tight-binding model of DNA: Spin filtering and chiral spin transport,” *Physical Review B*, vol. 93, p. 155436, apr 2016.
- [18] J. D. Torres, R. Hidalgo-Sacoto, S. Varela, and E. Medina, “Mechanically modulated spin-orbit couplings in oligopeptides,” *Phys. Rev. B*, vol. 102, p. 35426, jul 2020.
- [19] M. Geyer, R. Gutierrez, V. Mujica, and G. Cuniberti, “Chirality-Induced Spin Selectivity in a Coarse-Grained Tight-Binding Model for Helicene,” *The Journal of Physical Chemistry C*, vol. 123, pp. 27230–27241, nov 2019.
- [20] R. Naaman and D. H. Waldeck, “Chiral-Induced Spin Selectivity Effect,” *The Journal of Physical Chemistry Letters*, vol. 3, pp. 2178–2187, aug 2012.
- [21] Z. Xie, T. Z. Markus, S. R. Cohen, Z. Vager, R. Gutierrez, and R. Naaman, “Spin Specific Electron Conduction through DNA Oligomers,” *Nano Letters*, vol. 11, pp. 4652–4655, nov 2011.
- [22] M. S. Zöllner, S. Varela, E. Medina, V. Mujica, and C. Herrmann, “Insight into the Origin of Chiral-Induced Spin Selectivity from a Symmetry Analysis of Electronic Transmission,” *Journal of Chemical Theory and Computation*, vol. 16, pp. 2914–2929, may 2020.
- [23] S. V. Salazar, V. Mujica, and E. Medina, “Spin-orbit Coupling Modulation in DNA by Mechanical Deformations,” *CHIMIA International Journal for Chemistry*, vol. 72, pp. 411–417, jun 2018.
- [24] R. Naaman and D. H. Waldeck, “Chiral-Induced Spin Selectivity Effect,” *The Journal of Physical Chemistry Letters*, vol. 3, pp. 2178–2187, aug 2012.
- [25] R. Naaman and D. H. Waldeck, *The Chiral Induced Spin Selectivity (CISS) Effect*, ch. Chapter 6, pp. 235–270. World Scientific Publishing Co Pte Ltd, 2018.
- [26] H. Mouritsen, “Long-distance navigation and magnetoreception in migratory animals,” *Nature*, vol. 558, pp. 50–59, 2018.

-
- [27] J. Bojarinova, K. Kavokin, A. Pakhomov, R. Cherbunin, A. Anashina, M. Erokhina, M. Ershova, and N. Chernetsov, “Magnetic compass of garden warblers is not affected by oscillating magnetic fields applied to their eyes,” *Scientific Reports*, vol. 10, p. 3473, 2020.
- [28] R. Wiltschko, K. Stapput, P. Thalau, and W. Wiltschko, “Directional orientation of birds by the magnetic field under different light conditions,” *Journal of The Royal Society Interface*, vol. 7, pp. S163–S177, 2010.
- [29] H. G. Hiscock, H. Mouritsen, D. E. Manolopoulos, and P. J. Hore, “Disruption of Magnetic Compass Orientation in Migratory Birds by Radiofrequency Electromagnetic Fields,” *Biophysical Journal*, vol. 113, no. 7, pp. 1475–1484, 2017.
- [30] J. M. Matxain, J. M. Ugalde, V. Mujica, S. I. Allec, B. M. Wong, and D. Casanova, “Chirality Induced Spin Selectivity of Photoexcited Electrons in Carbon-Sulfur [n]Helicenes,” *ChemPhotoChem*, vol. 3, no. 9, pp. 770–777, 2019.
- [31] K. Burke, “Perspective on density functional theory,” *The Journal of Chemical Physics*, vol. 136, p. 150901, 4 2012. doi: 10.1063/1.4704546.
- [32] M. J. Kelly, “Applications of the Recursion Method to the Electronic Structure from an Atomic Point of View,” *Solid State Physics*, vol. 35, pp. 295–383, 1980.
- [33] F. Bloch, “Über die Quantenmechanik der Elektronen in Kristallgittern,” *Zeitschrift für Physik*, vol. 52, no. 7, pp. 555–600, 1929.
- [34] C. M. Goringe, D. R. Bowler, and E. Hernández, “Tight-binding modelling of materials,” *Reports on Progress in Physics*, vol. 60, no. 12, pp. 1447–1512, 1997.
- [35] V. Heine, “Electronic Structure from the Point of View of the Local Atomic Environment,” in *Solid State Physics* (H. Ehrenreich, F. Seitz, and D. Turnbull, eds.), vol. 35 of *Solid State Physics*, pp. 1–127, Academic Press, 1980.
- [36] R. Haydock, “The recursive solution of the Schrödinger equation,” *Computer Physics Communications*, vol. 20, no. 1, pp. 215–294, 1980.

-
- [37] T. Schena, *Tight-Binding Treatment of Complex Magnetic Structures in Low-Dimensional Systems*. PhD thesis, RWTH Aachen University, 2011.
- [38] H. Pastawski and E. Medina, “‘Tight Binding’ methods in quantum transport through molecules and small devices: From the coherent to the decoherent description,” *Revista Mexicana de Fisica*, vol. 47, pp. 1–23, 2001.
- [39] I. L. Schiff, *Quantum Mechanics*. New York: McGraw-Hill, 3rd ed., apr 1968.
- [40] E. Merzbacher, *Quantum mechanics*. Hoboken, NJ: Wiley, 3rd ed., 1998.
- [41] R. Eisberg, R. Resnick, and J. D. Sullivan, *Quantum Physics of Atoms, Molecules, Solids, Nuclei and Particles*, vol. 28. Wiley & Sons Ltd, 2nd ed., apr 1985.
- [42] C. Cohen-Tannoudji, B. Diu, and F. Laloë, *Quantum Mechanics Volume II: Angular Momentum, Spin, and Approximation Methods*. A Wiley-interscience publications, New York: Wiley-VCH, 2nd ed., 2019.
- [43] J. J. Sakurai and J. Napolitano, *Modern Quantum Mechanics*. Cambridge: Cambridge University Press, 2 ed., 2017.
- [44] P. Alken, E. Thébault, C. D. Beggan, H. Amit, J. Aubert, J. Baerenzung, T. N. Bondar, W. J. Brown, S. Califf, A. Chambodut, A. Chulliat, G. A. Cox, C. C. Finlay, A. Fournier, N. Gillet, A. Grayver, M. D. Hammer, M. Holschneider, L. Huder, G. Hulot, T. Jager, C. Kloss, M. Korte, W. Kuang, A. Kuvshinov, B. Langlais, J.-M. Léger, V. Lesur, P. W. Livermore, F. J. Lowes, S. Macmillan, W. Magnes, M. Mandea, S. Marsal, J. Matzka, M. C. Metman, T. Minami, A. Morschhauser, J. E. Mound, M. Nair, S. Nakano, N. Olsen, F. J. Pavón-Carrasco, V. G. Petrov, G. Ropp, M. Rother, T. J. Sabaka, S. Sanchez, D. Saturnino, N. R. Schnepf, X. Shen, C. Stolle, A. Tangborn, L. Tøffner-Clausen, H. Toh, J. M. Torta, J. Varner, F. Vervelidou, P. Vigneron, I. Wardinski, J. Wicht, A. Woods, Y. Yang, Z. Zeren, and B. Zhou, “International Geomagnetic Reference Field: the thirteenth generation,” *Earth, Planets and Space*, vol. 73, no. 1, p. 49, 2021.

- [45] C. Cattena, L. Fernández-Alcázar, R. Bustos-Marín, D. Nozaki, and H. Pastawski, “Generalized multi-terminal decoherent transport: recursive algorithms and applications to SASER and giant magnetoresistance,” *Journal of Physics: Condensed Matter*, vol. 26, no. 34, 2014.
- [46] U. Schollwöck, “The density-matrix renormalization group,” *Rev. Mod. Phys.*, vol. 77, no. 1, pp. 259–315, 2005.
- [47] S. Varela, B. Montañes, F. López, B. Berche, B. Guillot, V. Mujica, and E. Medina, “Intrinsic Rashba coupling due to hydrogen bonding in DNA,” *The Journal of Chemical Physics*, vol. 151, p. 125102, sep 2019.
- [48] R. P. Feynman, “Space-Time Approach to Non-Relativistic Quantum Mechanics,” *Reviews of Modern Physics*, vol. 20, pp. 367–387, apr 1948.
- [49] Y. Aharonov and M. Vardi, “Meaning of an individual "Feynman path",” *Physical Review D*, vol. 21, pp. 2235–2240, apr 1980.
- [50] R. D. Mattuck, *A Guide to Feynman Diagrams in the Many-body Problem*. Dover Books on Physics Series, Dover Publications, 2nd ed., 1992.
- [51] Y. Shen and C.-F. Chen, “Helicenes: Synthesis and Applications,” *Chemical Reviews*, vol. 112, pp. 1463–1535, mar 2012.
- [52] A. Tsuneya, “Spin-Orbit Interaction in Carbon Nanotubes,” *Journal of the Physical Society of Japan*, vol. 69, no. 6, pp. 1757–1763, 2000.
- [53] A. Szabo and N. S. Ostlund, *Modern Quantum Chemistry: Introduction to Advanced Electronic Structure Theory*. Mineola: Dover Publications, Inc., first ed., 1996.
- [54] L. W. Molenkamp, G. Schmidt, and G. E. W. Bauer, “Rashba Hamiltonian and electron transport,” *Physical Review B*, vol. 64, p. 6, 2001.
- [55] C. H. Edwards, “Euclidean Space and Linear Mappings,” in *Advanced Calculus of Several Variables*, ch. 1, pp. 1–55, Academic Press, 1973.